NASA TECHNICAL NOTE

NASA TN D-4730

NASA TN D-4730

M-1 INJECTOR DEVELOPMENT — PHILOSOPHY AND IMPLEMENTATION

by Walter F. Dankhoff, Irving A. Johnsen, E. William Conrad, and William A. Tomazic

Lewis Research Center
Cleveland, Ohio

NATIONAL AERONAUTICS AND SPACE ADMINISTRATION • WASHINGTON, D. C. • AUGUST 1968

M-1 INJECTOR DEVELOPMENT - PHILOSOPHY AND IMPLEMENTATION

By Walter F. Dankhoff, Irving A. Johnsen, E. William Conrad, and William A. Tomazic

Lewis Research Center
Cleveland, Ohio

NATIONAL AERONAUTICS AND SPACE ADMINISTRATION

For sale by the Clearinghouse for Federal Scientific and Technical Information
Springfield, Virginia 22151 – CFSTI price $3.00

ABSTRACT

The M-1 injector design was a cooperative effort between Aerojet-General Corporation and Lewis Research Center to achieve high performance with completely stable operation. The approach was based on the technology already established in the RL-10 and J-2 engine development programs, supplemented with the latest data obtained at NASA-Lewis. Scall-scale tests were conducted to verify design concepts prior to incorporation into the full-scale hardware. Full-scale injector testing demonstrated that the design goals were achieved.

M-1 INJECTOR DEVELOPMENT - PHILOSOPHY AND IMPLEMENTATION

by Walter F. Dankhoff, Irving A. Johnsen, E. William Conrad, and William A. Tomazic

Lewis Research Center

SUMMARY

The M-1 injector was designed with the intent of circumventing the normal "cut-and try" development route by using all pertinent technology to design a satisfactory end product, that is, an injector that combines high performance, stable operation, and durability. The approach employed was to make full use of all existing information and experience, to provide additional data (as required) through subscale testing, to employ analytical simulations to provide guidance, and to utilize the highest level of technical competence available to arrive at final design decisions.

Full-scale injector testing demonstrated that the design goals were achieved. Combustion efficiency was 96 percent at rated conditions. Vacuum specific impulse, extrapolated from the basic test data was 429.5 pounds force second per pound mass (4212 N-sec/kg), which is equivalent to the PFRT engine specification. The injector was highly resistant to both hydraulic and acoustic instabilities. No instabilities of any sort were encountered at rated conditions. Low-level chugging occurred during the start transient only. Acoustic instability was encountered only when the hydrogen inlet temperature was dropped significantly below the engine operating value. The injector, the baffle, and the ablative chamber showed excellent integrity. Prolonged testing was possible without equipment repair or replacement.

INTRODUCTION

Injector development has historically been a prolonged, iterative process. The basic difficulty has been one of avoiding combustion instability, while at the same time obtaining high combustion performance. The problem has become more severe as engine size has increased. Lack of basic knowledge on instability, its prevention, and cure has gen-

erally forced injector development along the tortuous path of cut-and-try, with its associated long delays and high costs. The injector becomes the pacing item in the engine development and the remainder of the program marks time and accrues costs until the injector problem is solved. In some engine programs, as many as 100 full-scale injector configurations have been investigated before a satisfactory design was achieved. Although the initial efforts on the M-1 program included several injector types, a decision was made during the restructuring of the program by NASA Lewis (in early 1963) to concentrate on the coaxial type of injector. This decision was based on the successful experience with the coaxial injector both at Lewis and in the RL-10 and J-2 development programs. The extremely long fabrication lead-times, however, made it necessary to retain one of the original injectors in the program to permit the timely initiation of test stand checkout.

In the period following the decision to utilize the coaxial injector on M-1, an intensive study was conducted to establish the exact design details of the injector to be incorporated into the engine. By this time, the successful development of the J-2 injector, as well as further research in the area, had led to the formulation of general design criteria for stable operation and high performance with hydrogen and oxygen. The problem of scaling results to the M-1 size remained. However, on the basis of the available information, a firm decision was made in late 1964 to pursue the "single-line" development of one of the designs. That injector incorporated fine elements (462 lb thrust per element); the choice was made on the basis that both high efficiency and stable performance could be achieved with this design.

TABLE I. - M-1 ENGINE SPECIFICATIONS

Thrust with 40 area ratio nozzle in vacuum, lb (N)	1 500 000 (6.67×10^6)
Chamber pressure at injector face, psia (N/m^2)	1040 (7.17×10^6)
Nozzle total pressure, psia (N/m^2)	985 (6.79×10^6)
Oxidant-fuel ratio, O/F	
Engine	5.0
Thrust chamber	5.5
Specific impulse (at PFRT), lbforce sec/lb mass (N-sec/kg)	
Engine	424 (4158)
Thrust chamber	429.4 (4221)
Hydrogen injection temperature, ^{o}R (^{o}K)	140 (78)

The design philosophy imposed in the development of the injector for the M-1 engine (table I) was, therefore, that rational design could be successfully employed for hydrogen-oxygen injectors and that extensive cut and try development was not necessary. The primary design objective was to achieve high performance (greater than 96-percent combustion efficiency) with completely stable operation. In addition, mechanical integrity and compatibility with the chamber were required.

In order to achieve these objectives, certain design philosophies were established and adopted: (1) The necessity for making proper engineering judgements based on the best available data at each step in the design process and (2) where data were not fully adequate, designing with sufficient margins to account for unknowns and to assure success. For example, all available techniques for eliminating high-frequency oscillations were considered and, as appropriate, incorporated into the M-1 design. The injector elements were designed to minimize or eliminate the acoustic driving mechanisms, and baffles were incoporated to damp any oscillations that might conceivably arise.

To carry out these design philosophies, an organizational structure was set up which allowed full utilization of the combined resources of the engine contractor (Aerojet-General Corporation) and the government manager (Lewis Research Center) in the most effective manner. The technical management group at Lewis was organized in parallel to the contractor's staff, thus, providing technical counterparts at the two installations. In addition, an inhouse research capability was provided at Lewis to quickly conduct subscale tests to verify design concepts prior to incorporation into full-scale hardware. This capability proved to be essential to timely and logical decision making.

The M-1 design utilized the technology already established in two previous hydrogen-oxygen engine development programs (the RL-10 and the J-2). This was supplemented by the latest research data relating to stability and performance, and verified by definitive subscale tests. Experts from other industrial and government organizations were consulted on specific technical aspects of the design. When the available information from all sources had been gathered and evaluated, final decisions were made by the technical team. Four specific areas, the injector proper, the injector baffles, the ablative chamber, and the ignition or start system were all subjected to this extensive design analysis and subscale testing prior to commitment to the full-scale design.

The design approach, the methods of implementation, and the actual hardware developed are described in this report. The four main technical areas (injector, baffles, chamber, and start system) are presented and discussed separately. In each of these major technical areas, the report attempts to summarize the information available to the technical team and the rationale and logic of the technical decisions that were made. The results of full-scale M-1 tests are then summarized and analyzed in terms of the design logic and the subscale test results. The advantages and limitations of subscale testing are discussed.

INJECTOR DEVELOPMENT

Background

An assessment of the current state of hydrogen-oxygen injector technology in late 1964 indicated that the J-2 injector design was the most appropriate base to use in designing the M-1 injector. The coaxial tube injector had by then become essentially standard for hydrogen-oxygen engines; both the RL-10 and J-2 used it. It was judged that acoustic instability was the most serious problem in the design of the huge M-1 injector, much more so than was the case for the smaller RL-10 and J-2 injectors. In the RL-10 development no acoustic instability was encountered, primarily because of its high hydrogen-injection temperature and small size; therefore, no useful data on suppression of acoustic instability were available. In the case of the larger J-2 engine, acoustic instability was encountered in the early phases of injector development, and techniques for its suppression were developed. The design criteria developed for the J-2 injector were utilized in the M-1 design. The problem of acoustic stability, of course, had to be integrated into the overall M-1 injector design along with consideration of hydraulic stability, combustion efficiency, and structural integrity.

Stability and performance. - It was indicated during the J-2 injector development that increasing hydrogen velocity (or momentum) and/or decreasing oxygen velocity resulted in greater stability. In designing coaxial injectors, this was accomplished by reducing the hydrogen-injection area and increasing the oxygen-injection area. Research at Lewis showed the ratio of hydrogen velocity to oxygen velocity to be a significant correlating parameter, with an increased velocity ratio resulting in greater stability. In evaluating the stability of a specific injector, hydrogen velocity was varied by varying the hydrogen-injection temperature. This approach to stability evaluation has been used extensively both at Lewis and at Rocketdyne for the J-2 development. The technique of operation used at Lewis was to begin at a hydrogen-injection temperature well above anticipated stability limits, then to ramp the temperature down. Figure 1, from reference 1, shows hydrogen temperature at transition from stable to unstable operation as a function of injection-area ratio. Regardless of hydrogen temperature or injection-area ratios, transition for this particular injector occurred at a velocity ratio of approximately 6.5. Higher velocity ratios resulted in stable operation, lower ratios in instability.

Another significant effect on stability and performance was that of recessing the oxygen tube below the plane of the injector face. The use of recessing was first demonstrated on the J-2 engine development program. For the J-2, a recess of 0.210 inch (0.0053 m) resulted in a 20° to 25° reduction in self-triggering temperature and a 2-percent increase in combustion performance. Figure 2 shows data obtained at Lewis for a 0.10-inch (0.0025-m) recess. The self-triggering temperature was improved by

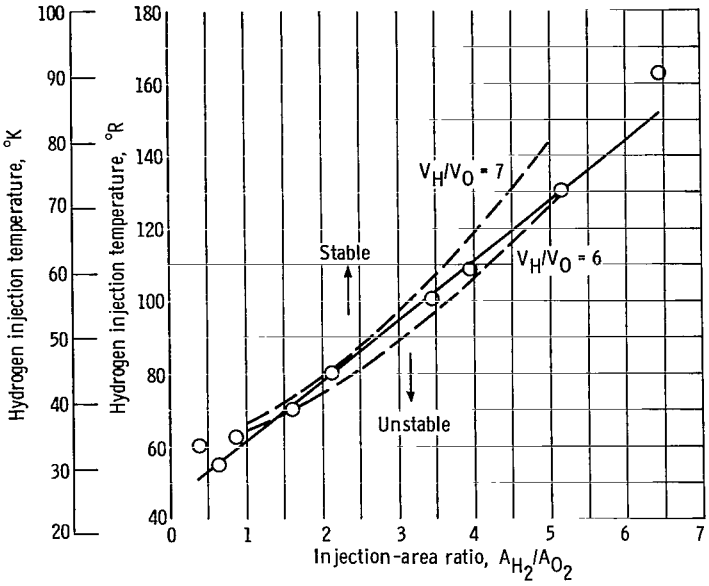

Figure 1. - Correlation of instability transition temperature with injection-area ratio for conventional concentric tube element injectors. Mixture ratio, 5.

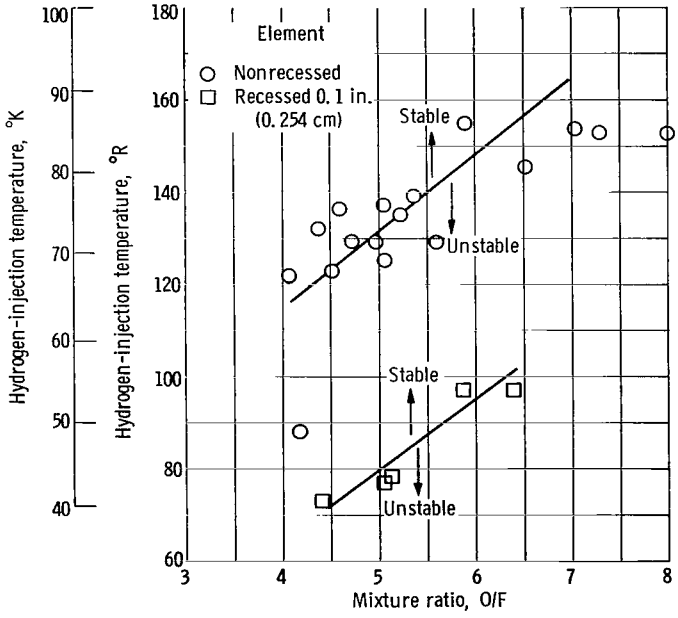

Figure 2. - Effect of oxidizer-tube recess on variation of instability transition temperature. Oxygen area, 0.89 square inch (5.74 cm^2); hydrogen area, 4.84 square inches (31.2 cm^2).

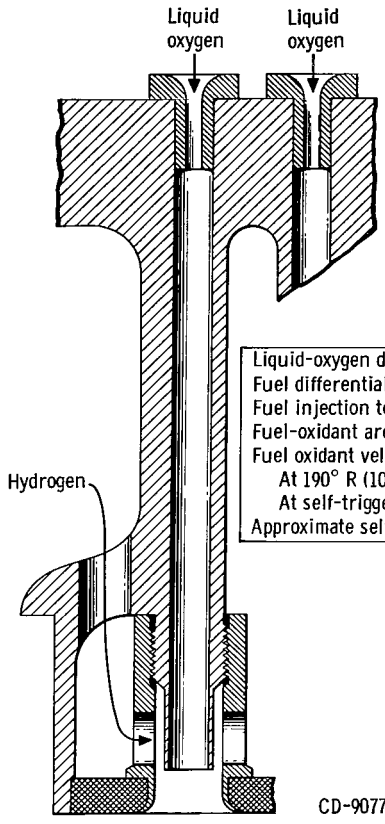

Liquid-oxygen differential pressure, psi (N/m^2)	170(1.17x10^6)
Fuel differential pressure, psi (N/m^2)	90(0.62x10^6)
Fuel injection temperature, °R (°K)	190(106° K)
Fuel-oxidant area ratio, A_f/A_{ox}	1.5
Fuel oxidant velocity ratio	
At 190° R (106° K)	12.5
At self-triggering temperature	2.6
Approximate self-triggering temperature, °R (°K)	70 (39)

Figure 3. - J-2 injector element. FRT prototype; low fuel pressure drop.

approximately 50° R (28° K) and performance by 3 to 4 percent. Recessing obviously has a powerful effect. Although the quantitative effect of recessing for a specific injector design cannot be accurately predicted, both the high velocity ratio and recess techniques enhance mixing and atomization of the coaxial propellant streams and thereby improve both stability and performance. The J-2 FRT injector (fig. 3) employed both effectively.

These two techniques were incorporated in the M-1 design. Hydrogen velocity was made as high as practical within the engine pressure budget. The fuel and oxidant discharge areas were chosen to provide a velocity ratio of approximately 18 at rated operating conditions. This is 40 percent higher than the J-2 velocity ratio at its operating point. An oxygen tube recess of 0.24 inch (0.0061 m), which is 0.030 inch (0.00076 m) deeper than that for the J-2, was used. No precise criteria for determining an optimum depth of recess were available at the time. Both available space and concern for excessive pressure drop or element erosion weighed against too deep a recess. Moreover, J-2 data indicated that the first 1/8 inch (0.0033 m) of recess produced the major effect.

Another key factor to be considered in designing the M-1 injector was the number of elements, or the thrust per element, to be used. Element size has been shown to have a significant effect on both performance (which generally increases with smaller elements) and acoustic stability (which generally decreases with smaller elements). The design problem was to select an element size which would give assurance of adequately high performance, yet not compromise stability. Injector bodies built to accommodate 1184 elements (1267 lb (5636 N) thrust per element) and 3248 elements (462 lb (2055 N) thrust per element) were available. Anticipated combustion efficiency as a function of element size was calculated using the vaporization criteria of reference 2 and the mixing criteria of reference 3. Calculations for the M-1 chamber and the type of element proposed indicated that vaporization would be essentially complete in 1/3 to 1/2 the length from the injector to the throat. Mixing could then be considered as the limiting criterion for performance. The simplified model for gas-phase turbulent diffusion in rocket combustors presented in reference 3 was used to estimate combustion efficiency for the M-1 as a function of element size (thrust per element). It was necessary to estimate the turbulence intensity to be expected in the M-1 because no adequate data were available. Turbulence for the J-2

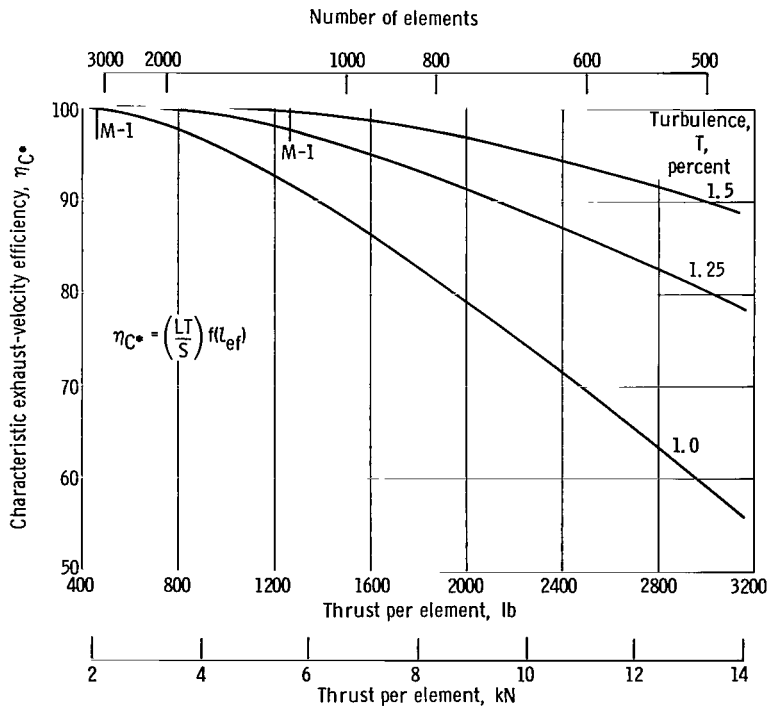

Figure 4. - Calculated characteristic-exhaust-velocity efficiency as function of thrust per element. Performance is mixing limited (based on these calculations). Vaporization is essentially 100 percent over spectrum of conditions.

chamber was calculated with an assumed basic combustion efficiency (without film cooling or other losses) of 98 to 100 percent. This turbulence intensity was then extrapolated to the M-1 by assuming similar injector characteristics and compensating for contraction ratio and chamber shape differences. It was concluded that an effective turbulence intensity for the M-1 lay between 1.0 and 1.5 percent of the free-stream velocity, with 1.25 percent taken as a most probable value. Figure 4 shows calculated maximum characteristic-velocity efficiency η_{C^*} as a function of element size and thrust per element for the M-1 chamber. An additional 2- to 3-percent loss in efficiency due to chamber film cooling, baffle cooling, nonideal mixture ratio, and flow distributions would be expected in a real injector. It is, therefore, indicated that the M-1 performance goals could not be achieved with an 1184-element injector unless the turbulence intensity was greater than 1.25 percent. On the other hand, the calculated efficiency for a 3248-element injector was high enough to meet the goal even at 1.0 percent turbulence. It was decided to use this injector in order to assure the desired high performance, and to rely on the specific element design (velocity ratio, recessing, etc.) and on added damping to provide stability.

Although acoustic mode instability was the prime concern in the element design, hydraulic instability or chugging obviously could not be overlooked as a problem. A single-dead-time model, as proposed in reference 4 (fig. 5(a)), was used to determine chugging instability boundaries for M-1 conditions. These boundaries are shown in figure 5(b) as a function of fuel and oxidant pressure drops and for dead times of 0.5 to 1.0 millisecond. Dead time for the M-1 injector was inferred from the data of reference 5 and was judged to be between 0.5 and 1.0 millisecond. The M-1 nominal operating point is for the injector mounted in a regenerative chamber with a 32-inch (0.81-m) diameter throat. It was felt that overall pressure drops of 400 psi (2.76×10^6 N/m^2) for oxygen and 200 psi (1.38×10^6 N/m^2) for fuel provided a satisfactory margin. Actual operation of the injector was carried out in an ablative chamber (see section ABLATIVE CHAMBER) with a 30-inch (0.76-m) diameter throat which resulted in lower injection-pressure drops. It was judged, based on past experience, that the selected single-dead-time analysis is somewhat pessimistic and that injector-pressure drops would still be sufficient to prevent chugging. In particular, the J-2 injector, which was quite similar in concept, supported this judgment. The J-2 injector had an oxygen pressure drop of 170 psi (1.17×10^6 N/m^2) (0.27 P_c), a fuel pressure drop of 90 psi (0.62×10^6 N/m^2) (0.14 P_c), and was invariably free from chugging, although a similar single-dead-time analysis indicated potential instability. Subscale tests of the M-1 configuration were also planned to corroborate this.

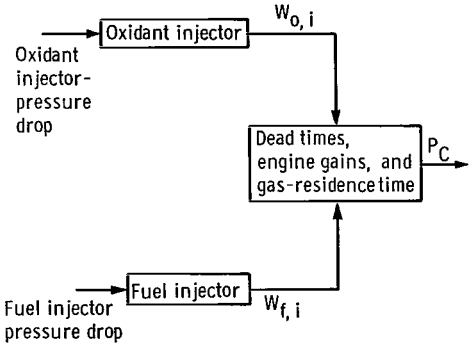

(a) Single-dead-time model.

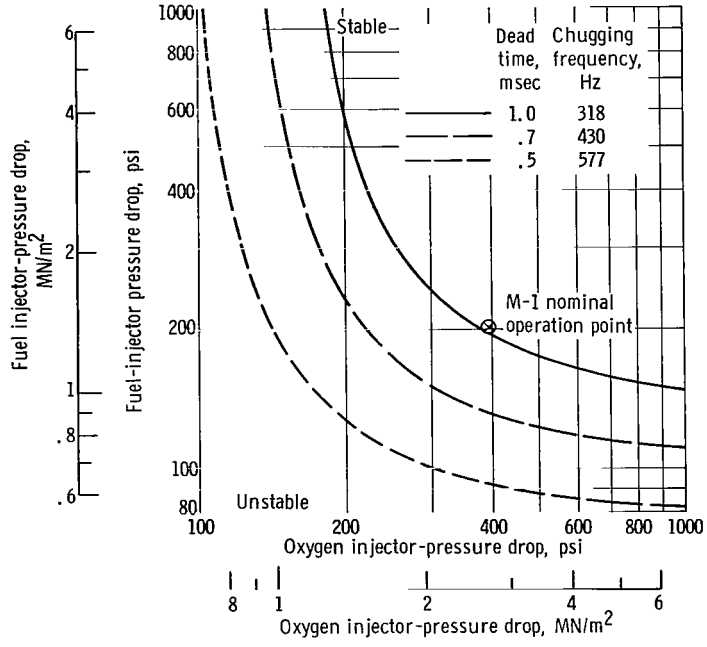

(b) Hydraulic instability boundaries.

Figure 5. - M-1 thrust-chamber instability boundaries based on single-dead-time model.

Injector	Number of elements	Element radius		Impingement length		Percent vaporized	Percent mixed	Percent vaporized and mixed
		in.	cm	in.	cm			
J-2	---	---	---	12	30.5	98.9	90.5	89.5
M-1	1184	---	---	9.5	24.1	93.6	34.0	31.8
	3248	19.57	49.7	9	22.9	98.2	51.5	50.6
		19.05	48.4	11.6	29.5	99.2	79.3	78.7
		18.52	47.0	14.4	36.6	99.6	90.7	90.4

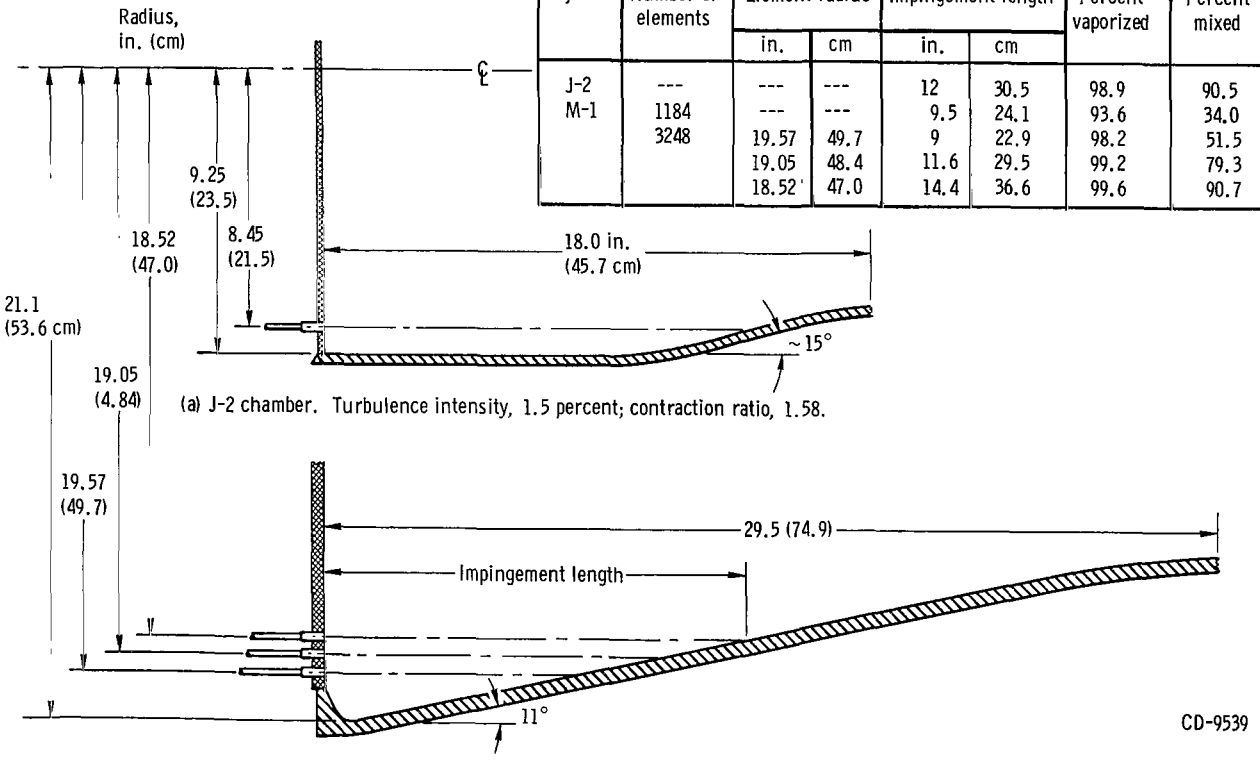

(a) J-2 chamber. Turbulence intensity, 1.5 percent; contraction ratio, 1.58.

(b) M-1 chamber. Turbulence intensity, 1.25 percent; contraction ratio, 1.74.

Figure 6. - Comparison of J-2 and M-1 regenerative chamber shape and wall impingement.

Mechanical integrity. - Another concern in the design of the injector was possible wall gouging due to impingement of oxygen flow on the chamber wall. Since the chamber was conical, impingement of axially directed injector streams occurred sooner than for a cylindrical chamber such as the J-2. Figure 6 shows a comparison of wall impingement for both the M-1 and J-2 regenerative chambers. The outermost J-2 element is alined so that unconsumed flow would strike the wall at a point 12 inches (0.3 m) downstream from the injector. Vaporization and mixing calculations similar to those made to decide on element size indicated that the oxygen was essentially all vaporized and 90 percent mixed with the hydrogen at this point. It would be expected that the residual free oxygen at the impingement point would not cause gouging. J-2 experience supports this. On the other hand, flow from the outer elements for the M-1 injector (if axial) would strike the wall largely vaporized, but only 50 percent mixed. It would be expected that gouging could occur. It was decided, therefore, to cant the outer four rows of elements inward at a 7^{o} angle to extend the wall impingement points far enough downstream to reduce the probability of gouging due to unconsumed oxygen. The 7^{o} angle cant was an approximate maximum dictated by injector dimensions. After the injector design had been committed and was in fabrication, it was decided to make the tests with an ablative liner in an uncooled chamber. This resulted in the chamber walls being nearly an inch (0.025 m) closer to the centerline than had been the case for the regenerative chamber. However, a reexamination of the wall impingement problem led to the conclusion that the 7^{o} cant should suffice to prevent gouging even for the ablative chamber.

A mechanical design study of the injector was made. In particular, the problem of attaching the oxygen-injection tubes to a structural backplate was studied in detail. The RL-10 injector body was machined from a single forging. The oxygen tubes were milled and trepanned out of the same parent stock as the backplate: The J-2 injector body was also machined from a single forging. However, an electrical discharge technique was developed to machine all the oxygen tubes at once. Both techniques provided for continuous parent metal between hydrogen and oxygen within the injector. This was felt to be the safest technique to avoid internal interpropellant leakage, which could result in extensive damage. The M-1 injector, however, was so large that it was impractical to machine the entire body including oxygen tubes from a single forging. Perhaps the most significant drawback to this approach would be the uncertainty in detecting internal flaws in so large a forging. A variety of potential techniques was studied. It was decided to furnace braze the oxygen tubes to the structural backplate. The joint had to be mechanically strong and leakproof even after numerous cycles of shock, vibration, and thermal loading. This was considered in the design of the joint itself and in specifying braze material and cycle. The joint design chosen is shown in figure 7. The threaded portion was

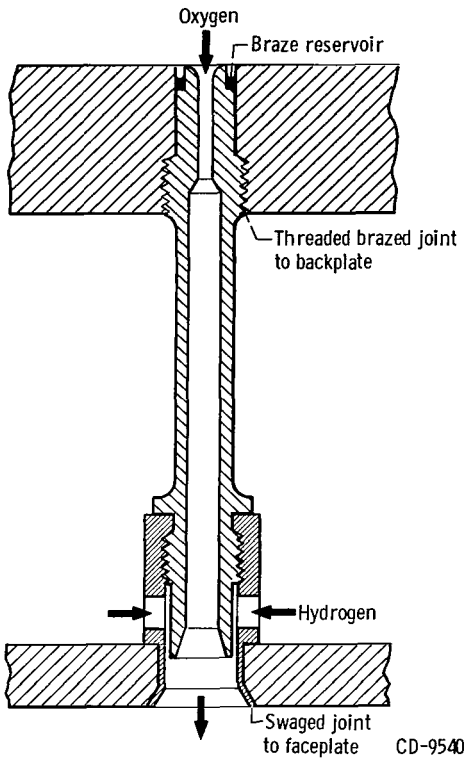

Figure 7. - Mechanical attachment of element to backplate and faceplate.

intended to add mechanical strength to the braze joint. Moreover, the threading would provide secure fixturing for the elements during the braze cycle. A reservoir was provided at each element to assure an adequate supply of braze to the joint. Copper was chosen as the braze material because of its toughness, ductility, and strength, particularly at cryogenic temperatures. In addition, copper braze is low in cost and allows for relatively simple rebraze cycles, if necessary.

Figure 7 shows an element fixed in place between the backplate, which faces the oxidizer dome, and the faceplate, which faces the combustion chamber. The attachment to the backplate is a brazed joint; the attachment to the faceplate is made by threading on a fuel sleeve which is in turn swaged into the faceplate. As was the practice for both the RL-10 and J-2 injectors, the faceplate was Rigimesh, a porous material which allows very simple and effective transpiration cooling of the face.

Cooling. - Design calculations for the M-1 regenerative chamber led to the decision to use 3 percent of the fuel for film cooling at the injector end. This was done to reduce coolant tube wall temperatures and to ameliorate the effects of any local injector anoma-

lies which might cause tube damage. The J-2 uses about 2 percent of the fuel for this purpose and, also, to reduce total-fuel pressure drop by reducing the fuel temperature rise. Both J-2 and Lewis data on the effect of film cooling on combustion performance indicated that a loss of up to about 1/4 percent in combustion efficiency would result from each percent of film cooling. It was expected the total fuel devoted to film and transpiration cooling - approximately 3 percent through the faceplate, 3 percent around the periphery of the injector, and 4 to 6 percent through the baffles - could reduce performance as much as 3 percent from the base performance level, which mixing and vaporization considerations indicate to be close to 100 percent of the theoretical value.

Subscale Testing

Assimilation of the injector information from the J-2 engine program coupled with more recent information from studies at Lewis and Aerojet (refs. 6 and 7) led to a series of six preliminary injector-element designs. These designs were carefully evaluated with regard to performance and stability goals, structural integrity, and ease of fabrication. As a result of the evaluation, two basic element designs (fine and coarse) were chosen. On the basis of broad general experience and trends indicated in the literature, the fine element was expected to produce higher efficiency, but the coarse was expected to provide more assurance of stable engine operation. The fine-element design, nevertheless, was expected to be stable inasmuch as it incorporated a high hydrogen-to-oxygen velocity ratio, oxygen tube recess, and relatively high thrust per element. Note that even the fine elements (3248 required for the full-scale M-1) were quite large and flowed 33 percent more propellant per element than those in the J-2 engine. Furthermore, in keeping with the overall program philosophy of achieving stable operation as well as high performance with the first injector configuration, the decision had been made to incorporate baffles on the injector faceplate as added ensurance that instability would not be a problem. The choice was, therefore, to use the fine elements in the M-1 engine.

To confirm the correctness of this design decision while the full-scale injector was in final design and fabrication, subscale test programs were conducted. Single-element tests were run at the engine manufacturer's plant to determine structural integrity and hydraulic characteristics, both with cold-flow and hot-firing conditions. The single-element thrust chamber used is shown in figure 8. Subscale tests were also conducted at the Lewis Research Center (see ref. 8) and are described briefly in the following paragraphs.

The subscale tests were conducted at a reduced-thrust level of 15 000 pounds (6.7×10^4 N), the maximum size compatible with the Rocket Engine Test Facility. This

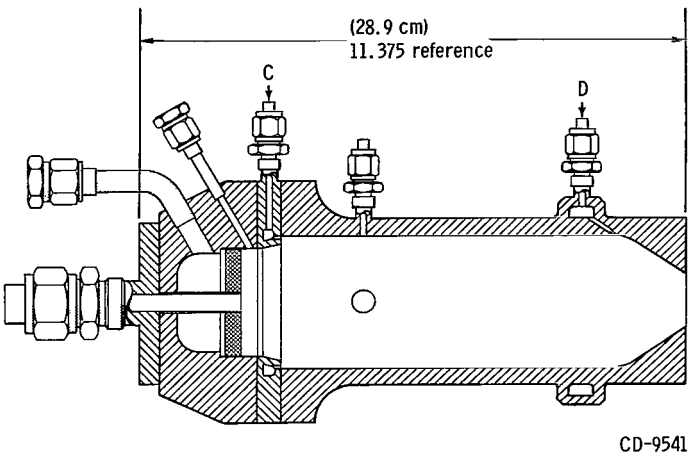

Figure 8. - Single-element thrust chamber.

limitation resulted in a subscale thrust chamber 5.39 inches (0.137 m) in diameter as compared with 42.0 inches (1.07 m) in full scale. The full-scale engine was duplicated exactly in the following aspects:

(1) Element size and detail

(2) Chamber pressure, 1040 psi (7.17×10^6 N/m^2)

(3) Element spacing

(4) Chamber length to throat, 29 inches (0.74 m)

(5) Contraction ratio, 1.7

It was recognized that precise scaling laws do not exist with regard to acoustic instability in rocket engines and, also, that large engines are more prone to screaming. Thus, despite the several measures used to attain stability with the fine elements in the full-scale engine, stability could not be guaranteed prior to test. Therefore, the coarse elements were also evaluated in the subscale program.

Engine. - The basic subscale engine was comprised of a concentric tube injector, a cylindrical heat-sink thrust chamber and a convergent-divergent heat-sink nozzle as illustrated in figure 9 (fine-element injector shown).

A heavy wall, carbon steel thrust chamber with a coating of 0.018 inch (0.00046 m) of zirconia on top of 0.012 inch (0.00030 m) of Nichrome was used. The nozzle converged from the chamber diameter of 5.39 inches (0.137 m) (42.0 in. (1.07 m) on M-1 engine) to a throat diameter of 4.15 inches (0.105 m) giving a contraction ratio of 1.7 (same as the M-1 engine). A short divergent section having an expansion ratio of 1.7 (40 on M-1 engine) was used because the tests were conducted in a sea-level rocket facility and because combustion performance was unaffected by the nozzle geometry down-

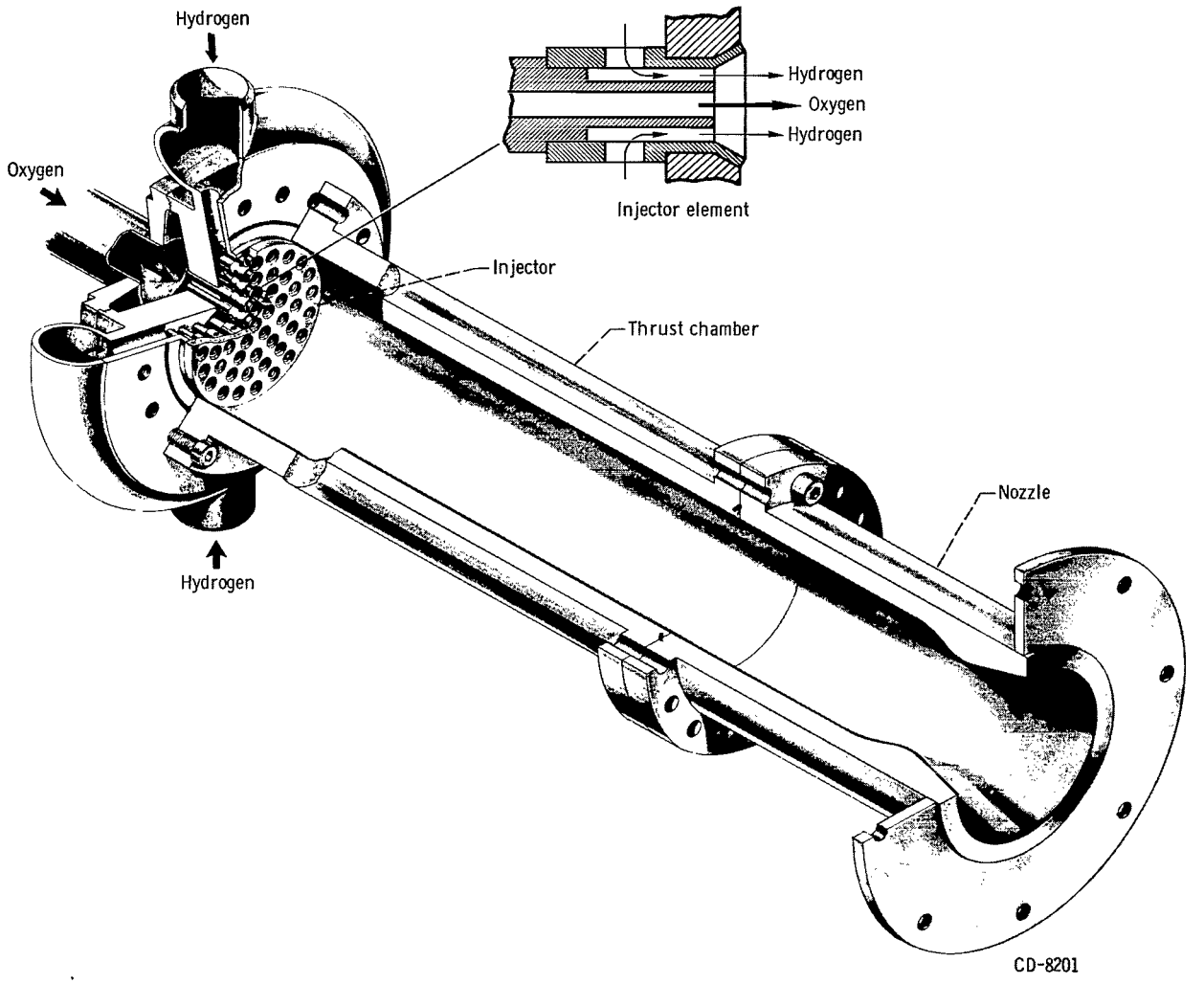

Figure 9. - Subscale engine.

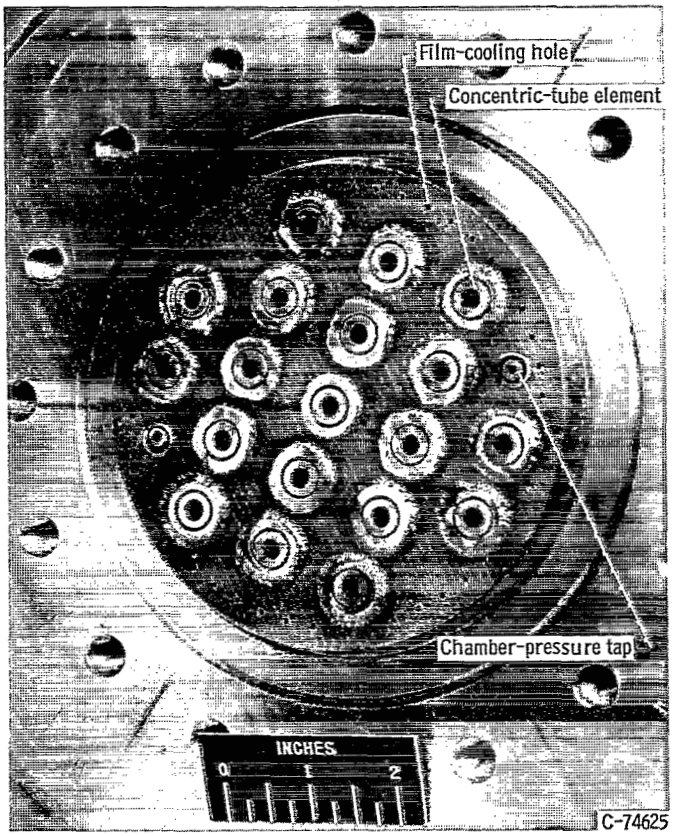

Figure 10. - Coarse-element injector. Thrust per element, 1267 pounds (5636 N).

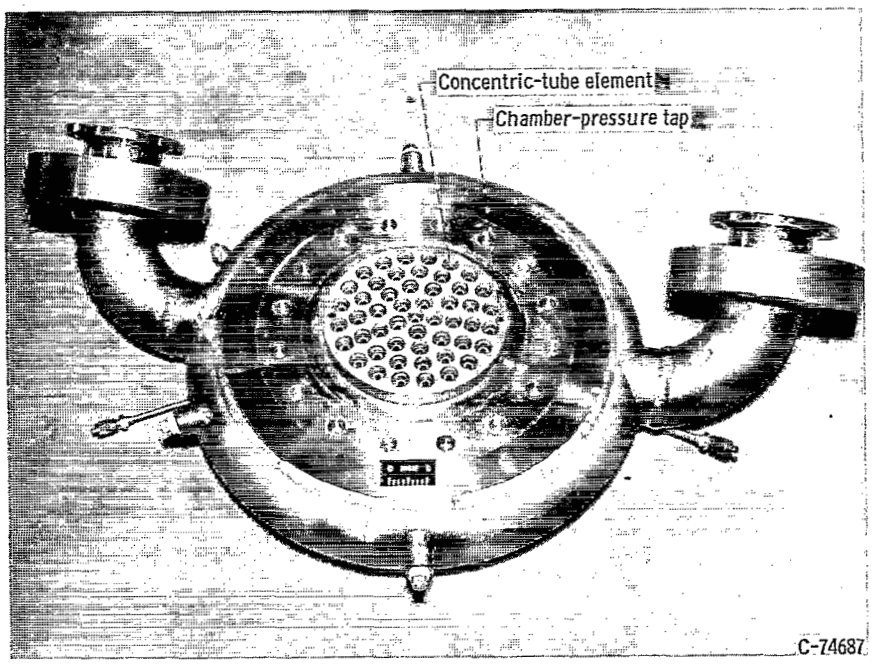

Figure 11. - Fine-element injector. Thrust per element, 462 pounds (2055 N).

stream of the throat. As indicated earlier, most of the testing was done using a 29-inch (0.74-m) long chamber; a 44-inch (1.1-m) chamber was used for some of these tests.

Faceplate views of a coarse injector (T/E = 1267 lbf (5636 N)) with 19 elements and a fine injector (T/E = 462 lbf (2055 N)) with 51 elements are shown in figures 10 and 11, respectively. The faceplate in each case was fabricated from 0.30-inch (0.0076-m) thick 347 stainless-steel Rigimesh having a permeability of 300 standard cubic feet per minute (0.14 m^3/sec) of air at a differential pressure of 20 psi (1.38×10^5 N/m^2). Note that, in figure 10, the 48 film cooling holes, 0.070 inch (0.0018 m) in diameter, are drilled through the Rigimesh face around the injector periphery. These holes were used for only one set of test data.

The injector elements, furnished by the M-1 engine manufacturer, were full-scale engine production elements. The fine-injector-element configurations had a design-point hydrogen-to-oxygen velocity ratio of about 18 at the design-point hydrogen-injection temperature of 140° R (78° K), while the coarse elements had a ratio of about 6.

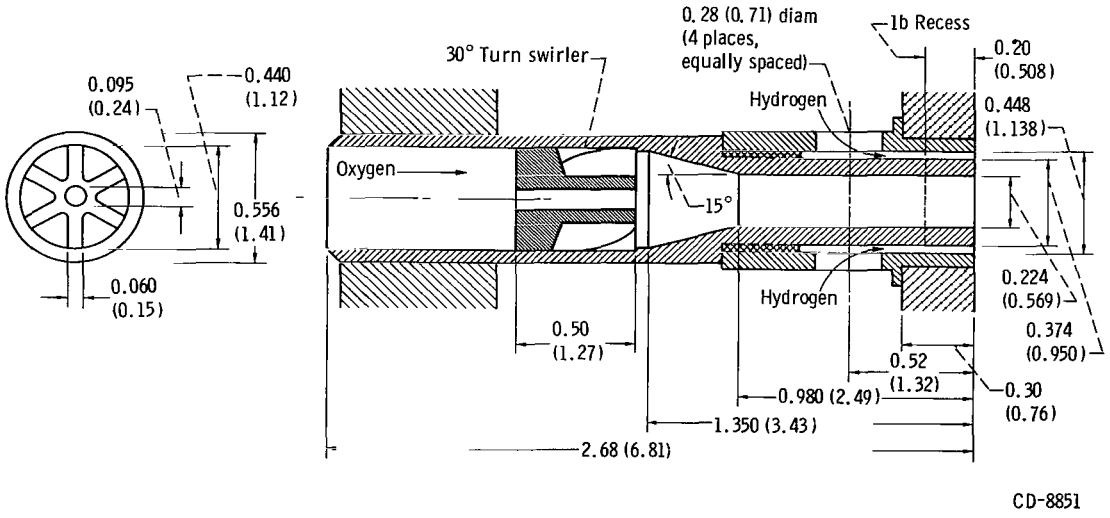

Figure 12. - Coarse-element injector. Configurations 1a and 1b are identical except for oxygen-tube recess shown for 1b. (All linear dimensions are in inches (cm).)

A cross-sectional view of the coarse-injector-element configurations is shown in figure 12. Both configurations 1a and 1b have a 30° swirler and were identical with the exception that the oxygen tube is recessed 0.2 inch (0.0051 m) in configuration 1b.

Cross-sectional views of the four fine-injector-element configurations are shown in figure 13 where their differences may be noted. Just a few tests had been made with configuration 2a when it was decided that the oxygen tube entrance should be modified to

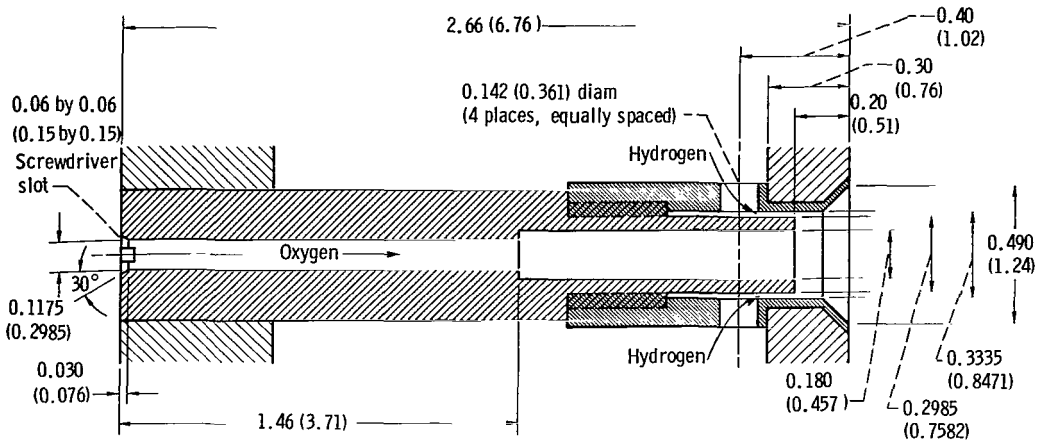

(a) Configuration 2a.

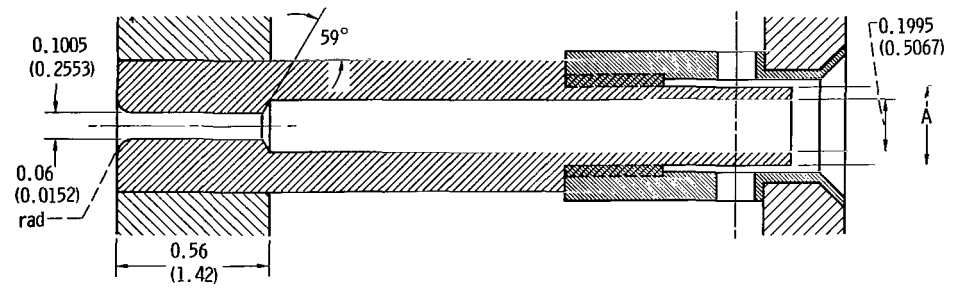

(b) Configurations 2b and 2c. Diameter A is 0.2985 inch (0.7582 cm) for 2b and 0.290 inch (0.737 cm) for 2c.

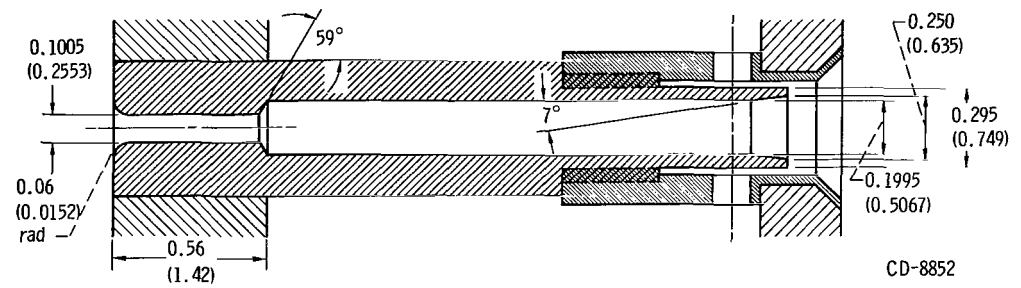

(c) Configuration 2d.

Figure 13. - Fine-element injectors. (All linear dimensions are in inches (cm).)

incorporate a greater restriction as a deterent to chugging instability. A slight enlargement in the oxygen tube exit area was also incorporated in the second fine-injector-element configuration, 2b. Configuration 2c differed from 2b in the oxygen tube exit outer diameter, which was slightly smaller, resulting in a slightly larger hydrogen exit area. The oxygen tube of configuration 2c was taper reamed at a 7^{o} angle resulting in configuration 2d shown in figure 13(c). Note that the taper reaming of the assembled injector resulted in slight flaring of the tube exit yielding a slightly larger outside diameter and, thus, decreasing the hydrogen area.

Performance. - Performance values given herein are based on chamber-pressure measurements corrected for momentum losses and are shown in terms of characteristic-velocity efficiency (η_{C*}) expressed as a percentage of the theoretical equilibrium value from reference 9. Unless otherwise noted, performance plots contain only data points with an oxidant-to-fuel mixture ratio (O/F) of 5.5±1.0. Nominal M-1 operating conditions are a chamber pressure of 1040 psia (7.17×10^6 N/m^2) at 5.5 O/F and a hydrogen-injection temperature of 140° R (78° K).

Performance of the coarse-injector-element configurations as a function of hydrogen-injection temperature is presented in figure 14. No appreciable η_{C*} differ-

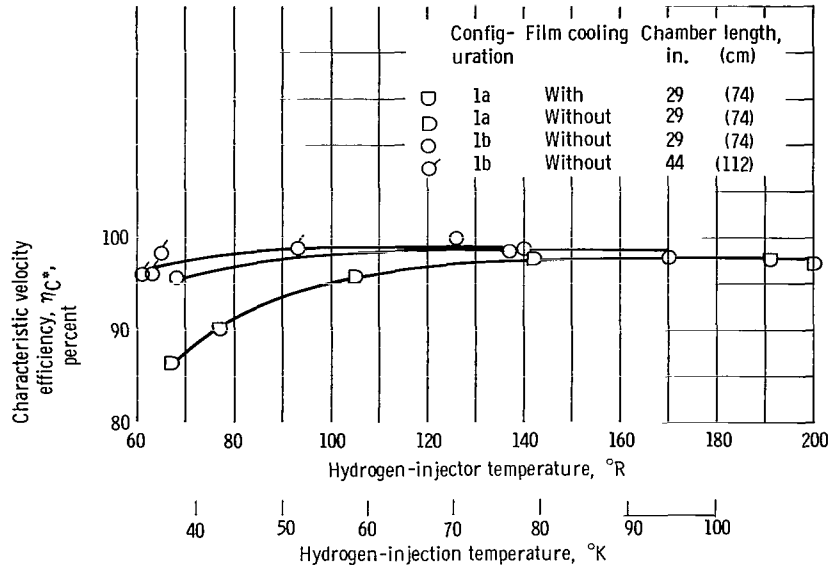

Figure 14. - Coarse-injector performance. Chamber pressure at injector face, 1040±100 psia ($7.17\times10^6\pm0.689\times10^6$ N/m^2); mixture ratio, 5.5±1.0.

ence between configuration 1a with 17-percent film cooling and the same configuration without film cooling was found, although the minimal number of data points does not make this a firm conclusion. Configuration 1a does exhibit an appreciable drop in efficiency as hydrogen-injection temperature is decreased below the design value of 140° R (78° K). The 0.2-inch (0.0051-m) recess of the oxygen tube, configuration 1b, appears to slightly increase the efficiency at 140° R (78° K) from 97.5 percent to almost 99 percent. Recessing definitely decreased the performance drop-off with decreasing hydrogen-injection temperature because the efficiency of the recessed configuration dropped only about 1 percentage point at a temperature of 95° R (53° K) compared with 3 percentage points for the flush configuration. The difference in efficiency increased to approximately 8 percent at 68° R (38° K). Increasing chamber length from 29 inches (0.74 m) to

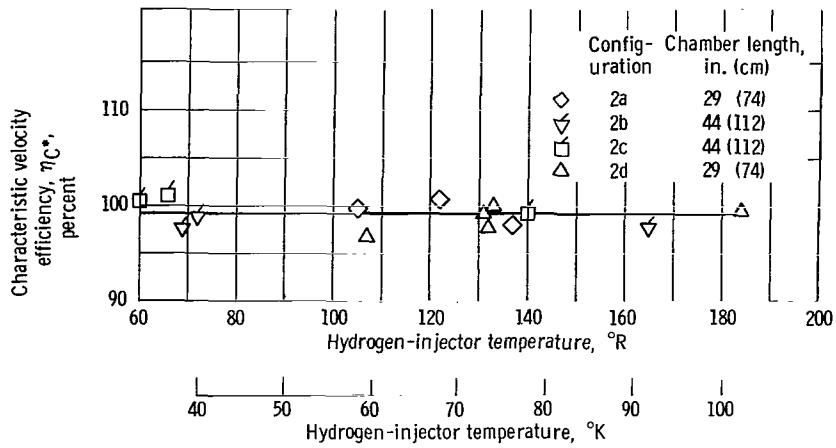

Figure 15. - Fine-injector performance. Chamber pressure at injector face, 1040±100 psia (7.17x10^6±0.689x10^6 N/m^2); mixture ratio, 5.5±1.0; no film cooling.

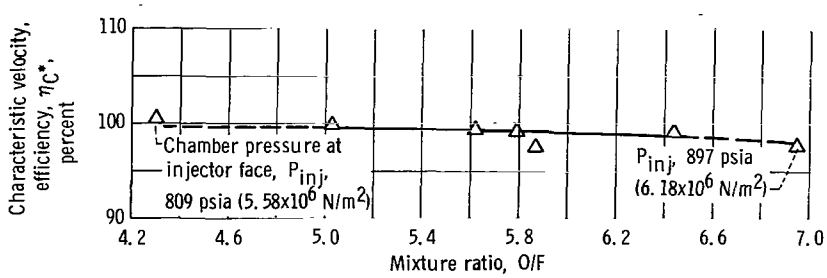

Figure 16. - Configuration 2d performance. Nominal chamber pressure at injector face, 1040 psia (7.17x10^6 N/m^2); nominal hydrogen-injector temperature, 140° R (78° K).

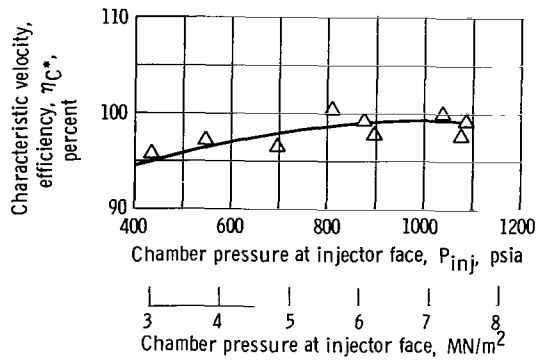

Figure 17. - Chamber-pressure effect on performance of configuration 2d. Nominal hydrogen-injector temperature, 140° R (78° K).

44 inches (1.1 m) with the recessed configuration further increased efficiency at low temperatures by 2 percent.

The effect of hydrogen-injection temperature on the efficiency of the fine-element injector is shown in figure 15. The efficiency is approximately 99 percent for all four fine-element configurations. Figures 14 and 15 indicate that the fine-element injector is slightly superior in performance. This advantage is only a fraction of a percent at 140° R (78° K), but is greater at lower hydrogen temperatures.

Element configuration 2d was the one that had been chosen for the full-scale injector tests. Variations in operating parameters were then made in these subscale tests in order to obtain more performance information for this element. The effect of mixture ratio on η_{C*} of configuration 2d is presented in figure 16 for a nominal 140° R (78° K) hydrogen-injection temperature and 1040-psia (7.17×10^6-N/m^2) chamber pressure. Two data points at lower chamber pressure are used to extrapolate the curve to mixture ratio extremes. The line drawn through the data points indicates a 1-percent drop-off in efficiency from 4.5 to 6.5 O/F. Presented in figure 17 is the effect of chamber pressure on η_{C*} of configuration 2d at a nominal hydrogen-injection temperature of 140° R (78° K). The line drawn through the data points shows a drop in efficiency from 99 at a chamber pressure of 900 psia (6.2×10^6 N/m^2) to 95 at a pressure of 440 psia (3.0×10^6 N/m^2).

In regard to performance, therefore, the subscale tests indicated a high level of efficiency with a very slight edge in performance for the fine elements at design conditions. In addition, it was shown that the effect of small departures from nominal chamber pressure, mixture ratio, or hydrogen temperature, should have no serious effects on performance.

Stability. - Neither chugging nor screaming was encountered at or near the nominal M-1 operating conditions with any of the element configurations. Chugging was encountered during many start transients; however, such occurrence is of little consequence. Five runs were made using coarse-element injectors; chugging occurred with chamber pressures in the range 65 to 836 psi (0.45×10^6 to 5.76×10^6 N/m^2). Again, this is well below design and not, therefore, regarded as serious.

In the total of 66 runs comprising the subscale program, longitudinal mode acoustic instability of low amplitude was observed twice. Both instances were with the 44-inch (1.1-m) chamber, which was used in an attempt to model the frequency of the full-scale tangential oscillation with a longitudinal oscillation in the subscale chamber. The instabilities occurred at test conditions far from the anticipated operating conditions. Details of this work are presented in reference 8. No conclusions can be drawn from the results because it is not possible to relate quantitatively the occurrence of a longitudinal mode of acoustic instability in the subscale test (44-in. (1.1-m) length) to the possibility of tangential instability in the full-scale chamber (42-in. (1.07-m) diameter).

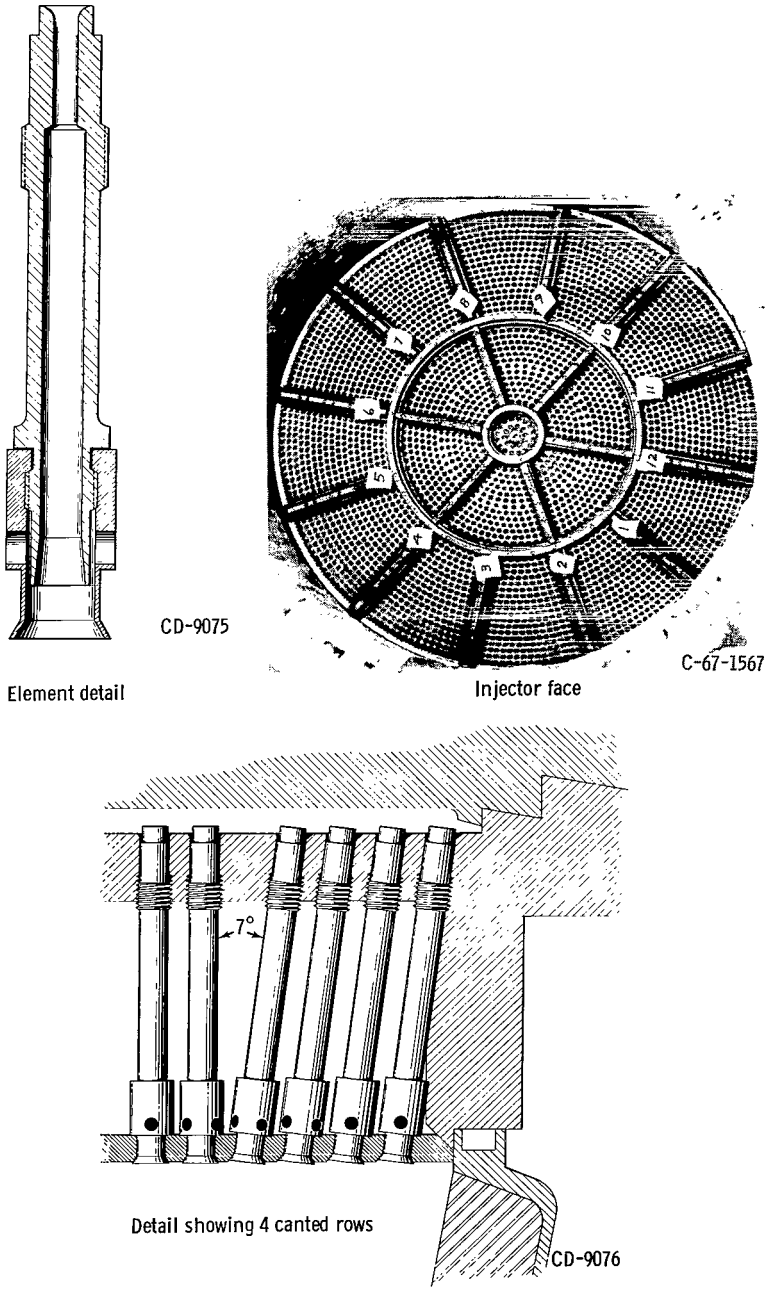

Figure 18. - Full-scale injector.

Full-Scale Testing

The full-scale injector layout is shown in figure 18. As shown, the chosen baffle layout produced 19 separate injection compartments. The total number of identical elements required to produce the full-scale thrust was 3248. As discussed earlier, the four outer rows of elements were canted toward the chamber center line at 7° to move the point of impingement with the 11° convergent chamber farther downstream. Some of the details of the full-scale injector are presented in the following table:

Fuel sleeve inside diameter, in. (cm)	0.333 (0.846)
Oxidant-tube outside diameter, in. (cm)	0.290 (0.737)
Oxidant-tube inside diameter at exit, in. (cm)	0.250 (0.635)
Oxidant-tube recess, in. (cm)	0.24 (0.61)
Fuel exit area, in.^{2} (m^2)	0.02104 (1.36×10^{-5})
Oxidant exit area, in.^{2} (m^2)	0.0491 (3.17×10^{-5})
Oxidant orifice diameter, in. (cm)	0.0994 to 0.1005 (0.252 to 0.255)
Fuel differential pressure, psi (N/m^2)	140 (0.97×10^6)
Oxidant differential pressure, psi (N/m^2)	360 (2.5×10^6)
Fuel density, lb mass/ft^3 (kg/m^3)	1.48 (23.7)
Oxidant density, lb mass/ft^3 (kg/m^3)	70.0 (1120)
Fuel mass flow per element, lb mass/sec (kg/sec)	0.133 (0.0603)
Oxidant mass flow per element, lb mass/sec (kg/sec)	0.839 (0.381)
Fuel-oxidant area ratio	0.429
Fuel velocity, ft/sec (m/sec)	615 (187)
Oxidant velocity, ft/sec (m/sec)	35.2 (10.7)
Fuel-oxidant velocity ratio	17.5

Performance. - The first goal of the full-scale test effort was to determine performance. The tests were made in an ablative-lined chamber with a 2.08 expansion ratio. Thrust, weight flows, pressures, and temperatures were measured to determine performance. Specific impulse and C* were derived from the basic data. Characteristic-velocity was calculated from both measured specific impulse, using an analytically derived thrust coefficient, and from basic parameters (chamber pressure, mass flow, and throat area) with analytical correction made for nonisentropic acceleration (momentum pressure loss). The two values agreed within 1/2 percent, with the C* derived from specific impulse being the lower. Figure 19 shows combustion characteristic-velocity efficiency as a function of mixture ratio for both the full-scale and subscale testing. Combustion efficiency was calculated using the C* derived from specific impulse and the theoretical C* for 140° R (78° K) hydrogen inlet temperature.

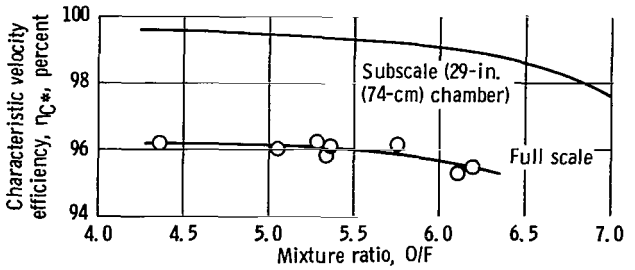

Figure 19. - M-1 thrust-chamber characteristic velocity efficiency against mixture ratio. Thrust-chamber design mixture ratio, 5.5; chamber pressure, 1100 psia (7.6×10^6 N/m^2 abs).

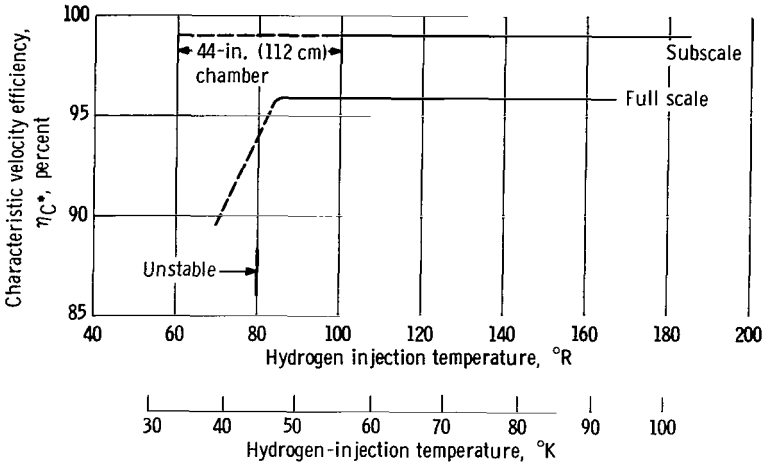

Figure 20. - M-1 thrust-chamber characteristic velocity efficiency against hydrogen-injection temperature. Mixture ratio, 5.5±1.0; design injectio temperature, 140° R (78° K).

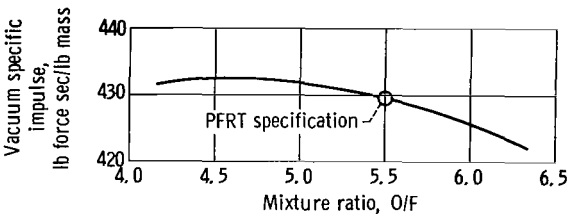

Figure 21. - M-1 thrust-chamber vacuum specific impulse against mixture ratio. Chamber pressure, 1100 psia (7.6×10^6 N/m^2), area ratio nozzle, 40.0; hydrogen-injection temperature, 140° R (78° K).

The full-scale performance of 5.5 O/F was 96 percent of theoretical with a slight increase at lower O/F's and a dropoff at higher O/F's. This performance level met the original goals prescribed for this injector. The subscale data show the same trend with O/F, but they are about 3 percent higher. The subscale injector data define a base or ideal level of performance. Deviation from this ideal, as noted earlier, was caused by two factors. First, the full-scale injector devoted approximately 5 percent of its fuel flow to baffle cooling and 3 percent to peripheral film cooling. Data obtained at Lewis and at Rocketdyne on the J-2 program indicate a performance loss of approximately 1 percent for each 4 percent of film cooling. This implies a performance loss for the M-1 injector of approximately 2 percent. Second, 748 elements (23 percent) adjacent to the baffles were modified (see baffle section) in order to protect the baffles. Although a precise evaluation of this effect was not made during subscale testing, it is conceivable that a percent or more loss could be attributed to this "dimpling".

Figure 20 shows η_{C*} as a function of hydrogen-injection temperature. Both the full-scale and subscale injectors maintain constant efficiency down to low hydrogen temperatures, probably because of the high hydrogen-oxygen velocity ratio. Other work at Lewis has shown that a high velocity ratio is helpful in maintaining a high efficiency level with decreasing hydrogen temperature (ref. 1). The full-scale performance did drop precipitously approximately 5° before the onset of acoustic instability as hydrogen temperature was ramped downward from rated conditions to determine the self-triggering point. This coincided essentially with the beginning of a metastable condition prior to full-blown instability.

The performance data obtained at sea level were extrapolated to vacuum conditions with an assumed area ratio nozzle of 40. This was done using thrust coefficients determined with a nozzle performance evaluation computer program developed by United Aircraft Corporation. Figure 21 shows the results obtained. The performance at 5.5 O/F (the thrust chamber O/F at engine rated conditions) is 429.5 pound force-second per pound mass (4212 N-sec/kg), which is equivalent to the contract specification for PFRT.

Stability. - The full-scale injector operated stably under all conditions of mainstage, normal operation. Chugging was experienced during the early phases of the staged start transient when injection pressure drops were very low. Chugging pressure amplitudes were approximately 45 psi (0.31×10^6 N/m^2) peak-to-peak during the first phase of the start at 300 psi (2.1×10^6 N/m^2) chamber pressure. The amplitude fell to about 23 psi (0.16×10^6 N/m^2) during the second phase of the start at 450 psi (3.1×10^6 N/m^2) and chugging disappeared completely as the chamber pressure rose. This is substantially in keeping with the subscale results and indicates a quite stable system.

These data were compared with stability limits derived using a double dead-time chugging model (ref. 10). This model, for prediction of low-frequency stability for bipropellant rocket engines, includes a discrete vaporization time for each propellant plus

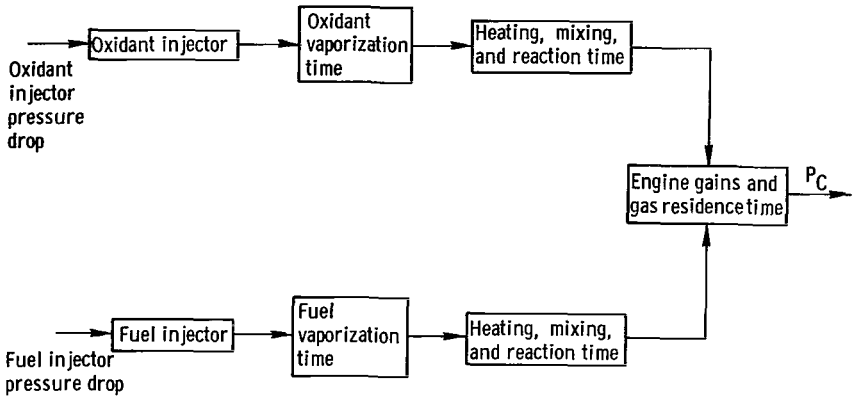

Figure 22. - Block diagram for double-dead-time stability limit model.

a mixing and reaction time common to both propellants. The block diagram for this model is shown in figure 22. Figure 23(a) shows the limits calculated for the first phase of the start. Oxygen vaporization time was calculated using the method of reference 2. Mixing time was inferred (using the calculated vaporization time and the total dead time derived from the chugging frequency) with approximately 0.1 millisecond best fitting the data. The test point is well into the unstable region as would be expected. Figure 23(b) shows the limits calculated for the second phase of the start. Two data points are shown: The first point was mildly unstable, near the boundary, and the second point, at higher chamber pressure and O/F, was stable. This transition appears to match the calculated stability boundary quite well. Figure 23(c) shows the boundaries calculated for the full-thrust condition. As can be seen, the operating point is well into the stable area - even when the hydrogen temperature is reduced to the self-triggering point.

The next phase of effort was to evaluate the acoustic stability characteristics of the injector. During the performance determination phase of the testing there was no indication of any acoustic instability. even during the start transient when temperatures dipped below 80° R (44° K) and mild chugging was in progress. The method used to induce acoustic instability was to reduce the hydrogen temperature as was done in the subscale testing. The results of this testing are shown in figure 24. Self-triggering temperature (temperature at onset of instability) varied from about 76° to 81° R (42° to 45° K) with the lower values occurring at low O/F's. During some of the later runs, the temperature was ramped back up after instability began. Return to stable operation occurred at approximately 100° R (55° K). These results indicate a substantial stability margin even under conditions of extreme perturbation, since the engine design operating temperature is 140° R (78° K). When instability was induced, the high-frequency pressure pickup data showed no definite mode of instability, which is in keeping with some experience with F-1 baffled injectors.

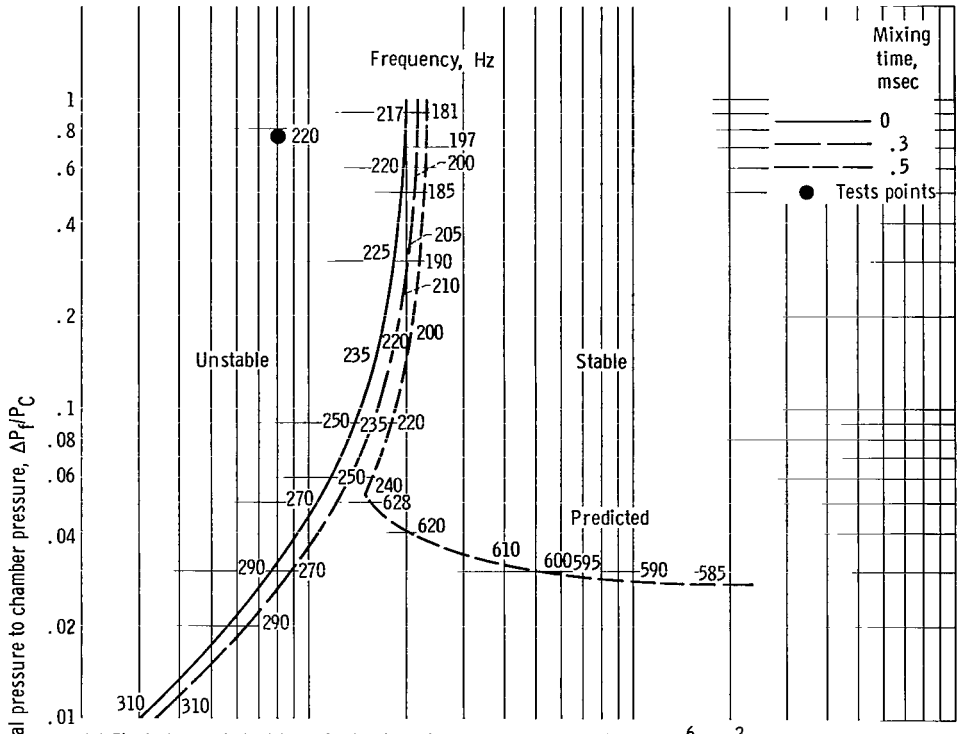

(a) First phase of start transient. Chamber pressure, 250 psi (1.72×10^6 N/m^2); mixture ratio, 1.5; vaporization time, 1.0 millisecond.

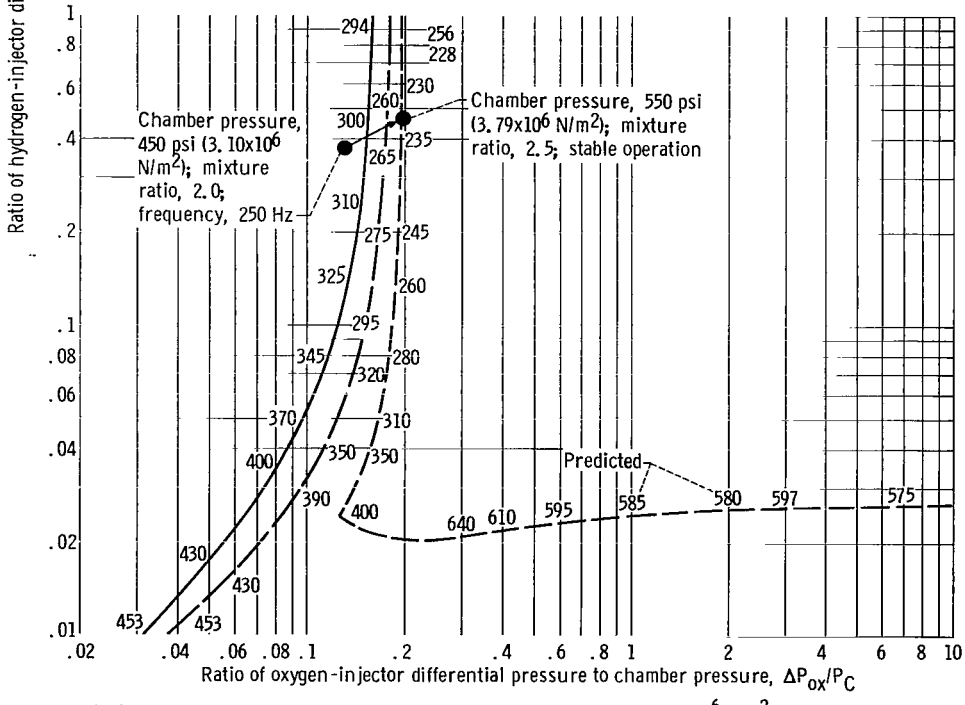

(b) Second phase of start transient. Chamber pressure, 450 psi (3.10×10^6 N/m^2); mixture ratio, 2.0; vaporization time, 1.0 millisecond.

Figure 23. - Hydraulic stability limits for M-1 injector based on double-dead-time model.

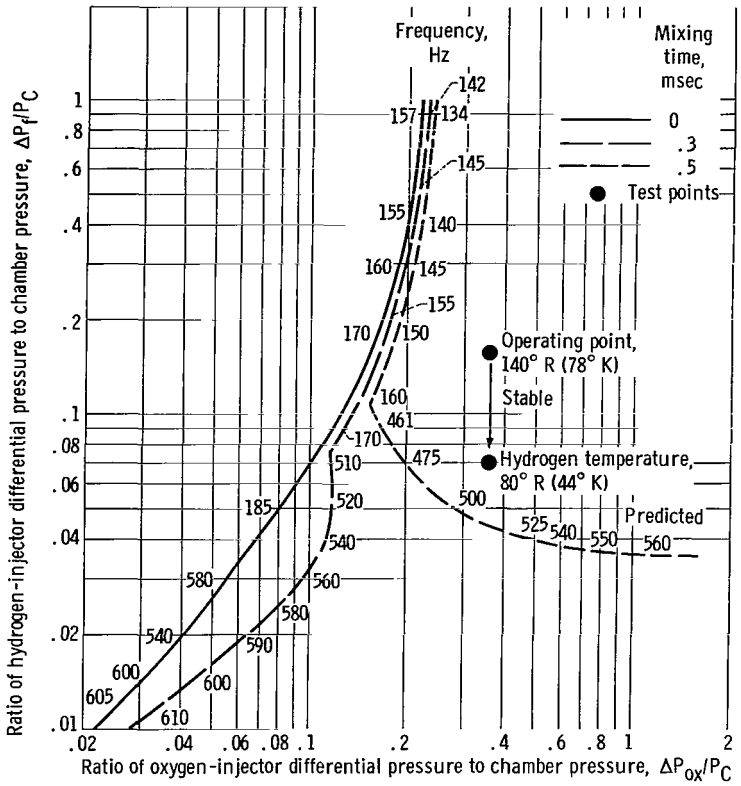

(c) Full thrust. Chamber pressure, 1058 psi (7.295×10^6 N/m^2) mixture ratio, 5.5; vaporization time, 2.4 seconds.

Figure 23. - Concluded.

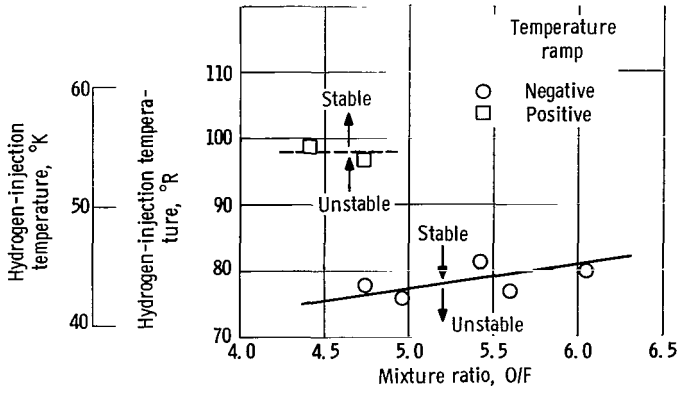

Figure 24. - M-1 thrust chamber combustion stability limits.

In summary, the original performance goals were met. The injector operated stably under normal conditions of operation and stability evaluation tests at lower hydrogen injection temperature showed considerable margin.

BAFFLE DEVELOPMENT

Background

Even though every attempt was made to design the injector utilizing the best information on design for stable operation, stability could not be guaranteed because of a lack of information on scaling. It was decided, therefore, that combustion baffles should be incorporated to further reduce the possibility of deleterious instability. The actual baffle configuration was designed at Aerojet General using the Sensitive Time Lag Theory developed by Crocco, et al., at Princeton University (ref. 11). Figure 25 shows the expec-

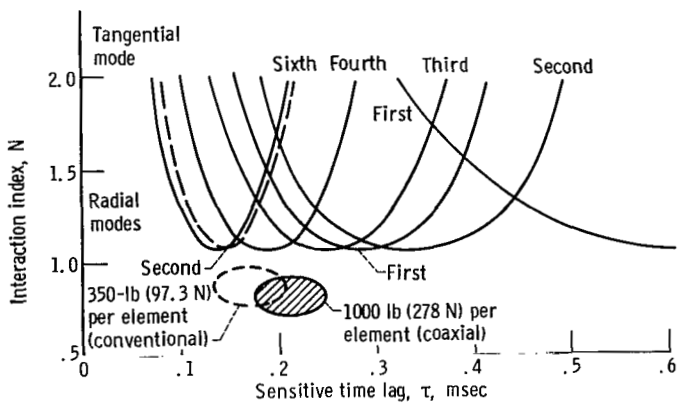

Figure 25. - M-1 thrust chamber instability zones without baffles.

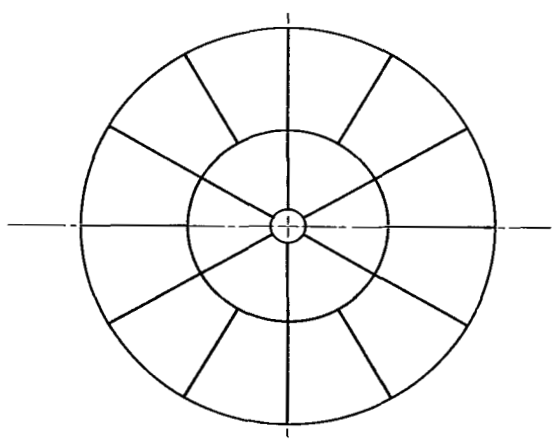

Figure 26. - Recommended baffle configuration.

ted interaction index N, and sensitive time lag τ zones for M-1 injectors in relation to various modes of instability for the M-1 chamber. The most likely modes of high-frequency instability are the third and fourth tangential, with frequencies in the range of 2000 to 3000 hertz. It was decided to provide protection against tangential modes lower than the sixth-tangential and the first-radial mode. Figure 26 shows the resulting baffle arrangement. Figure 27 shows a composite instability zone for the baffled injector, which includes the lowest radial (2nd) and tangential (6th) modes which can occur within the interbaffle spaces. The analysis is presented in detail in reference 12. This analy-

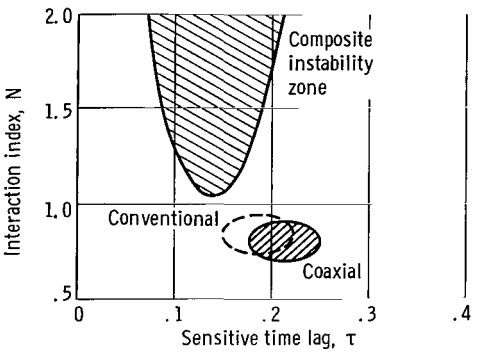

Figure 27. - Baffled chamber instability zone.

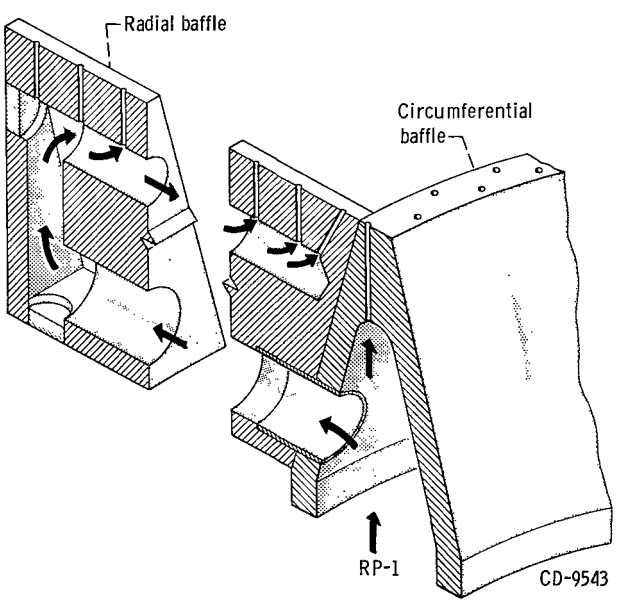

Figure 28. - F-1 Baffle coolant flow.

sis offered no specific guide as to baffle length; however, past experience led to a choice of 4 inches (0.1 m). It was felt that a 4-inch (0.1-m) baffle was long enough to be effective and not so long as to promote intercavity modes. This length was later reduced to $3\frac{1}{2}$ inches (0.089 m) because of cooling considerations.

It was also clear that the baffle must be both adequately and economically cooled. It must perform its function continuously and reliably without substantially compromising the injector performance. Four to six percent of the fuel was chosen as the maximum amount which could be devoted to baffle cooling without dropping the combustion performance below minimum goals. The most pertinent design information came from the F-1, J-2, and GEMSIP (Gemini Stability Improvement Program) programs. However, none of these designs were directly applicable to the M-1. The F-1 baffle was cooled convectively with the coolant fuel dumped at the baffle tip (fig. 28). The physical proportions were quite similar to those planned for M-1. However, the much greater heat flux of the M-1 would result in correspondingly greater temperature gradients through the metal and consequent excessive surface temperatures with this baffle configuration. A modification of this design, with the convective passages closer to the heated surfaces, might be more satisfactory. Another possible design would be to use film cooling in conjunction with convective cooling. Although the J-2 final injector was baffleless, some baffle development was done during the program. Of particular interest were the Rigimesh baffles which were tested (fig. 29) because this material had proven so effective in face cooling for hydrogen injectors. However, the few attempts made on the J-2 were unsuccessful. A review of the J-2 baffle design indicated that the failure may possibly have been due to basic structural inadequacy rather than overheating. Preliminary study indicated that a satisfactory Rigimesh baffle for the M-1 could be designed. The GEMSIP program evolved a regeneratively cooled baffle. This did not appear to be feasible or desirable for the M-1 because of its complexity and the pressure-drop requirements. However, the baffle heat-flux measurements made during this program were of considerable help in the preliminary design of M-1 baffles. Adequate experience and background to provide a firm basis for final design did not exist. Therefore, we decided to carry out a subscale test program to specifically develop the cooling design to be used for the M-1 injector baffle.

Subscale Testing

Formidable problems were faced in adequately cooling the baffles in the M-1 engine inasmuch as the local heat flux is estimated to be as high as 20 Btu per square inch per second (33×10^6 W/m^2). The use of closed-cycle internal regenerative cooling was ruled out because analysis of the engine cycle revealed that adequate coolant pressure drop could not be provided. Transpiration, film, and convective cooling techniques, were therefore, considered as well as various combinations. With these techniques, which ul-

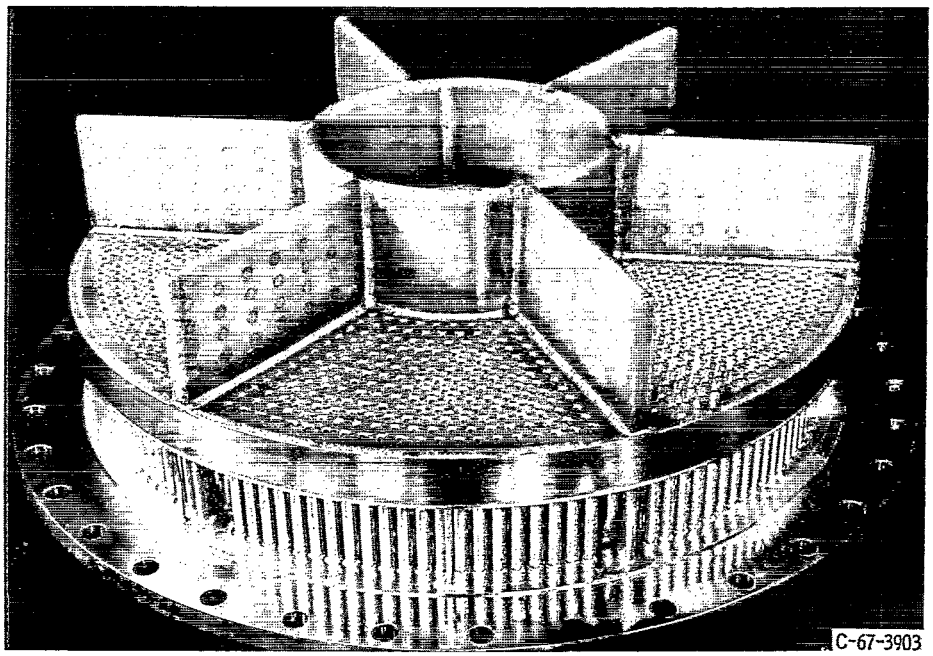

(a) Baffle before test.

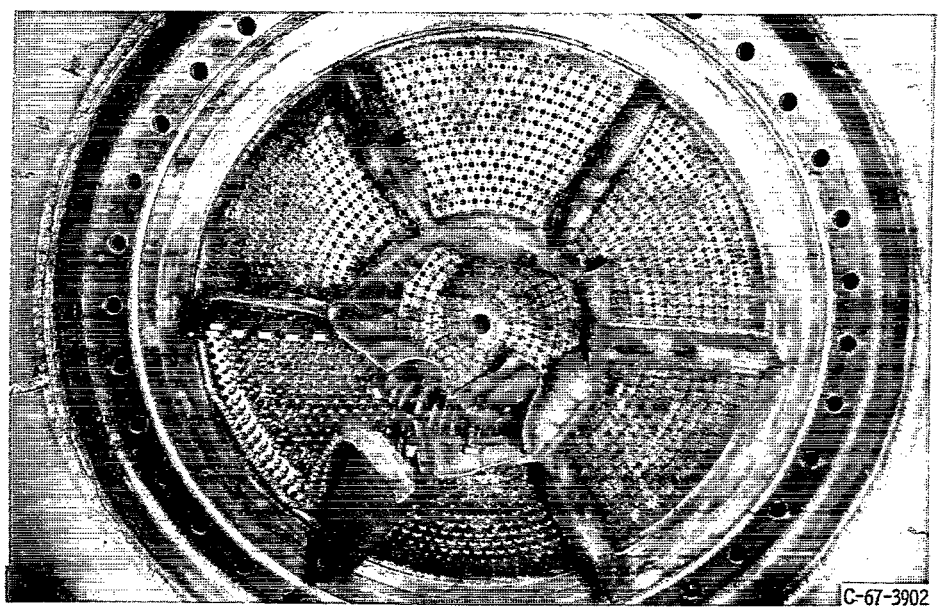

(b) Failed baffle.

Figure 29. - J-2 Rigimesh baffle.

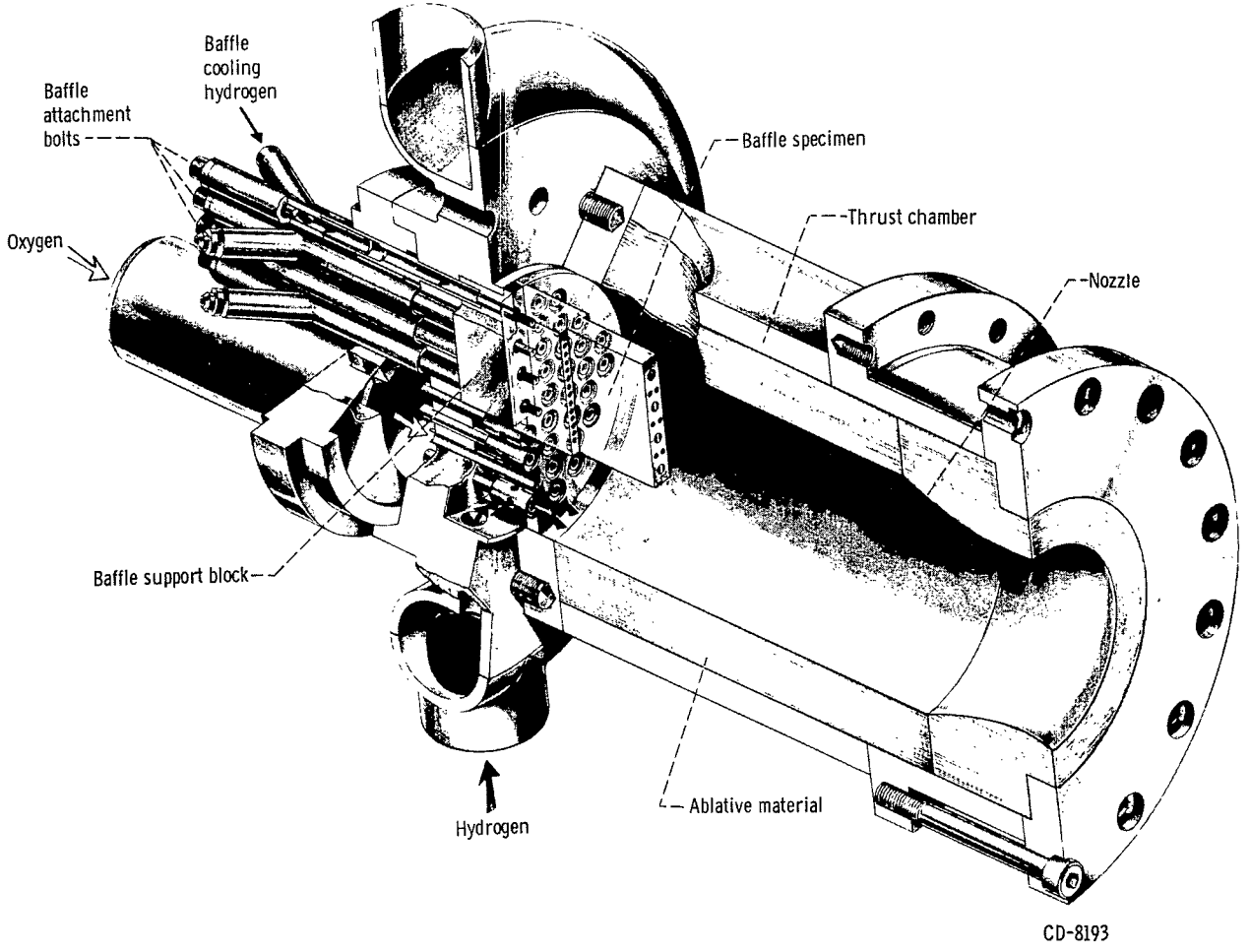

Figure 30. - Cutaway drawing of subscale engine.

timately dump their coolant into the combustion process in localized regions, it was estimated that only 4 percent of the total hydrogen could be used without excessive loss in specific impulse efficiency. This rather difficult position was further compounded by a lack of knowledge of the local heat-transfer environment near the injector, rendering precise calculations impossible.

Based on the foregoing, it was decided that baffle cooling tests were imperative. It was obvious, however, that such tests would be prohibitively expensive in full scale. A subscale test program was, therefore, conceived and conducted at Lewis using, with some modifications, the test set-up and hardware previously used for the injector-element investigation. The engine manufacturer contributed strongly to both the concepts and hardware aspects of the subscale program and also designed the full-scale injector to accommodate readily any baffle concept determined to be optimum in the subscale tests. The bolt-on design employed also provided a quick-change capability in the event of baffle deterioration during the full-scale test program. Shake table tests using the vibration spectrum predicted for the M-1 engine were carried out to verify the integrity of the bolt-on system prior to hot firing tests.

A cutaway drawing of the subscale engine test assembly is presented in figure 30. A separately controlled and metered flow of hydrogen at a temperature of close to 140° R (78° K) (M-1 design) was supplied through tubes to the base of the baffle. This deviated from the full-scale design where a separate baffle cooling system was not provided, and the coolant to the baffle was supplied from the hydrogen-injector cavity through holes

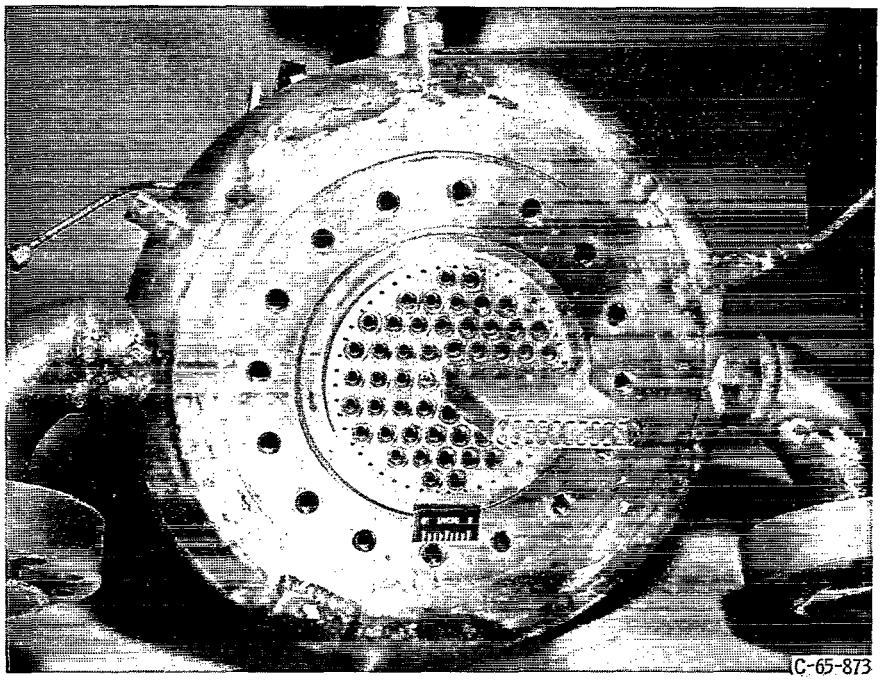

Figure 31. - View of injector with convectively-cooled baffle specimen installed.

drilled in the injector faceplate. A view of the subscale injector designed to accommodate the baffle test specimens is given in figure 31. The subscale tests were identical to full-scale in regard to:

(1) Chamber pressure
(2) Mixture ratio
(3) Contraction ratio
(4) Injector elements
(5) Element spacing with respect to baffle surfaces
(6) Element density

Accordingly and in view of the fact that subscale chamber diameter was not much smaller than the full-scale baffle cavities, it was felt that the axial heat flux distribution in the vicinity of the baffle was closely simulated.

As shown in figure 32, the subscale baffle specimens corresponded to a 2.85-inch (0.072-m) slice from one of the six inner spokes of the full-scale baffle. Twenty-five baffle specimens were evaluated by gradually reducing the baffle coolant flow until failure occurred. Detailed results are given in reference 13; only a few of the more significant findings are reported herein.

In the 25 specimens tested, only five basic cooling schemes were involved as indicated schematically in figure 33. The baffle types of primary interest herein are the transpiration (type A) and film and convection (type E). The other types were assessed as follows:

Type B - convectively cooled: All configurations showed some erosion near the tip but further development could probably achieve successful design.

Type C - reverse flow convection: Both 0.030 inch (0.00076 m) copper and stainless-steel (electrodeposited) shell configurations met design but showed incipient failure at 75 percent of design coolant flow. The type was discarded as too complex.

Type D - film cooled: Tip erosion of copper tang occurred with film-cooled lengths of 1.5 inches (0.038 m) or over.

Results obtained with the transpiration-cooled baffles are typified by the data of figure 34 where baffle differential pressure is plotted as a function of baffle coolant flow. The shaded region represents the range of values acceptable in the M-1 engine. It is seen that, as the baffle coolant flow was reduced from maximum, the baffle pressure drop at first decreased as expected, but then increased with further reductions of flow below about 0.27 pound per second (0.12 kg/sec). At about 0.15 pound per second (0.068 kg/sec), a maximum occurred followed by a decrease again toward the origin of the plot. As shown in reference 13, other designs of different porosity and construction did intercept the design region. Nevertheless, all the transpiration-cooled baffles were unacceptable because all exhibited the unexpected S-shaped characteristic shown in figure 34. Operation could occur at any of these regions (A, B, or C) for a given injector-pressure drop,

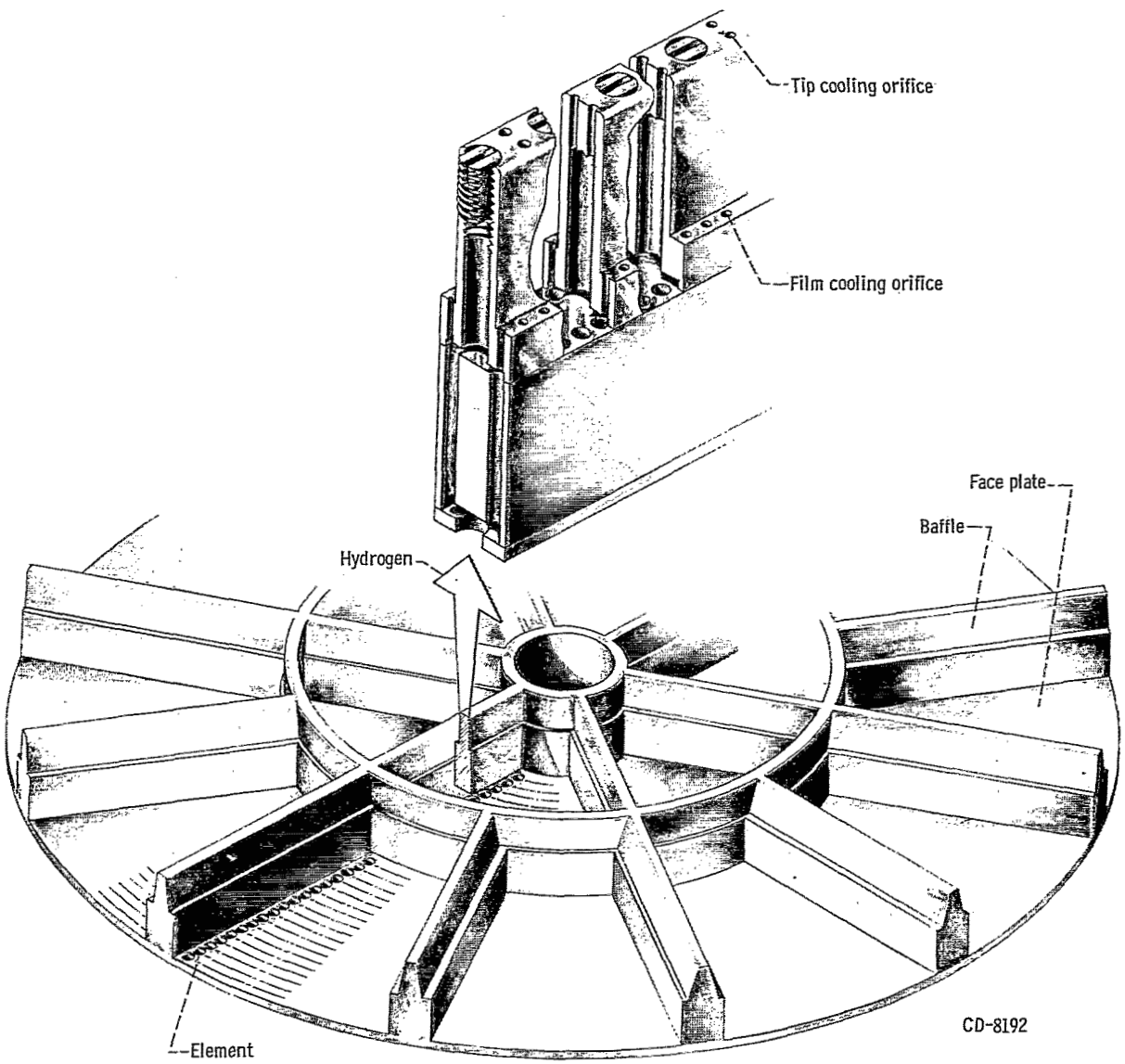

Figure 32. - Layout of full-scale M-1 engine baffle.

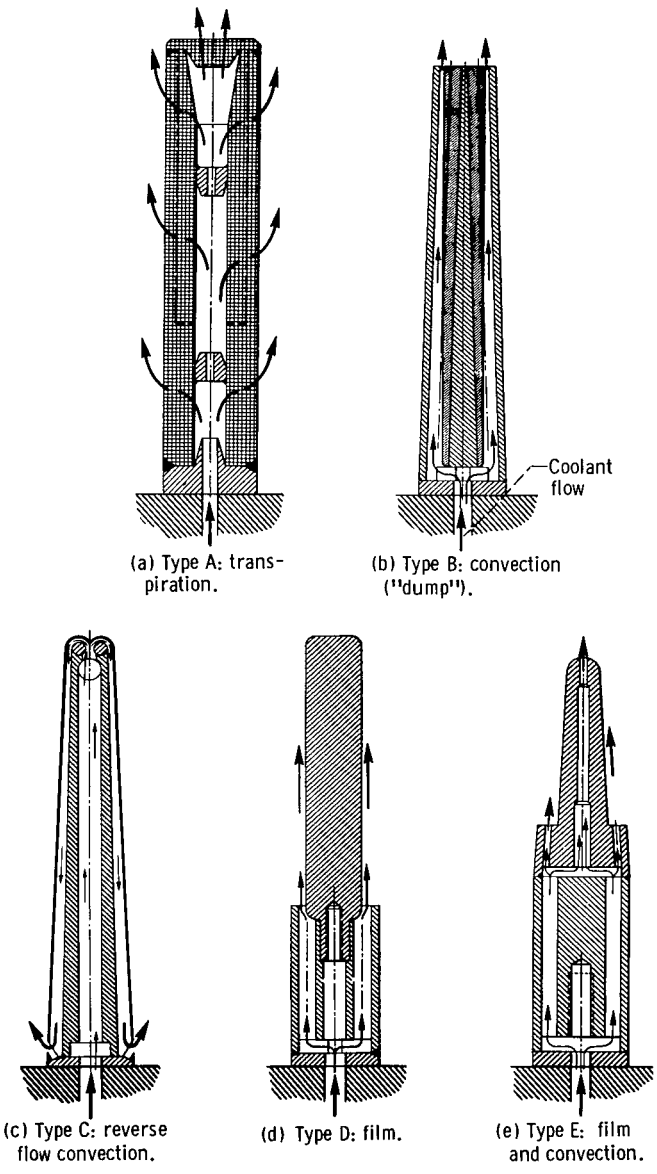

Figure 33. - Baffle cooling concepts investigated.

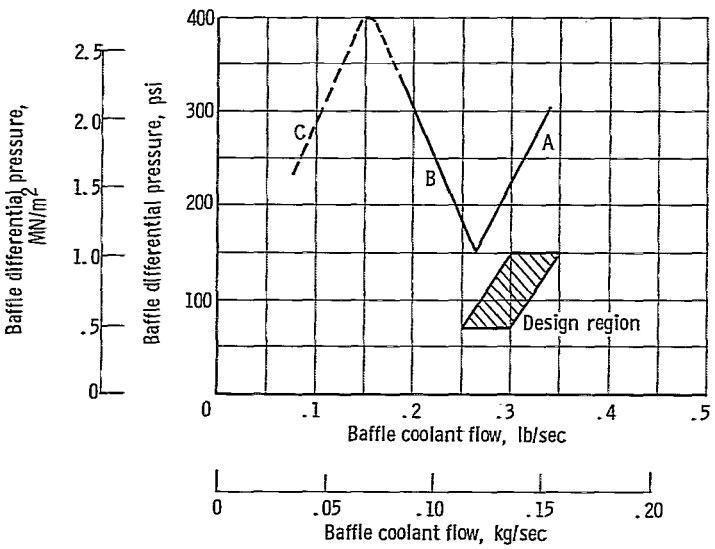

Figure 34. - Flow characteristics of transpiration cooled baffles. Baffle differential pressure correction to 140° R (78° K) baffle coolant inlet temperature.

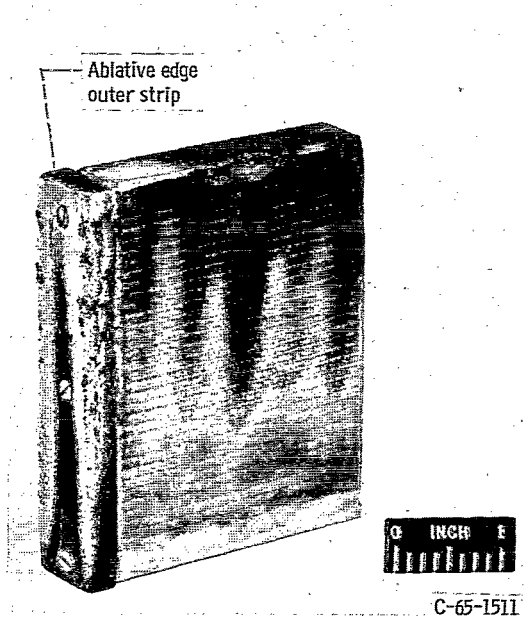

Figure 35. - Damage to transpiration-cooled baffle 4.

probably depending on the sequence of propellant flows during the complex conditions typical of engine start transients. Baffle integrity at B was marginal and damage occurred after two short runs at point C as shown in figure 35.

On the basis of a very cursory analysis, it appeared that the reversal (at 0.27 lbm/sec (0.12 kg/sec) in fig. 34) may be associated with sudden disruption of the cool boundary layer formed by the emerging coolant on the hot side of the baffle material. Disruption of this layer apparently allowed significant convective heat transfer to the baffle surfaces, causing the hydrogen to increase in temperature while passing through the porous material. Such heating would produce large reductions in hydrogen density, hence, higher velocities and increased pressure drop. Data similar to these had not been found in the prior literature possibly because experiments are not generally carried out to failure and the reversal point was not reached.

During the course of the subscale test program, it was postulated that the heat flux to the baffle could be reduced by modifying the injector elements adjacent to the baffle surfaces to decrease the mixture ratio near the baffle. To improve combustion stability, the standard injector elements (fig. 13(d)) incorporated a 7^{o} taper ream at the outlet of the oxidizer tubes. As shown in figure 36, the elements adjacent to one side of the baffle were dimpled (modification A) to direct the oxygen away from the baffle and, thus, reduce the local mixture ratio near the baffle. On the row on the other side of the baffle, the taper ream was eliminated (modification B) to reduce the spread of the oxygen jet with the same objective. The effects of these modifications were assessed qualitatively by visual observation of the post-run heat marking and the local tip erosion on a copper baffle. Both appeared to offer some benefit, but the dimpled configuration was slightly superior. Accordingly, the decision was made to use modification A in the full-scale injector on the elements adjacent to the baffles. Note that one oxidizer tube was plugged in the subscale injector at the edge of the baffle specimen to reduce heat flux to this edge which is not exposed in a full-scale engine (see fig. 32). Ablative strips were also used to avoid this problem on several baffles.

A number of type E baffle configurations employing combined convective and film cooling were investigated, with tip damage essentially eliminated at design conditions by detailed modifications. Postfire condition and flow characteristics of the final configuration are shown in figues 37 and 38. Details of this design, which was used for the full-scale M-1 engine, are shown by the inset of figure 32.

Full-Scale Testing

The final configuration of the full-scale baffle is shown in figure 32. It was made of 20 individual pieces; 12 outer legs, 6 inner legs, a 20-inch (0.51-m) diameter ring, and a

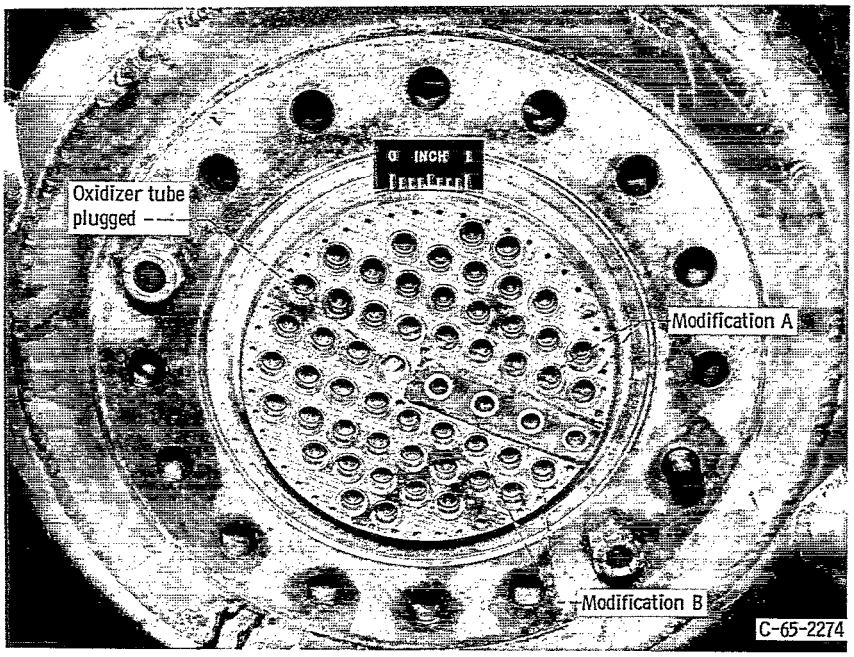

(a) View of injector showing relation of modified tubes A and B with respect to baffle.

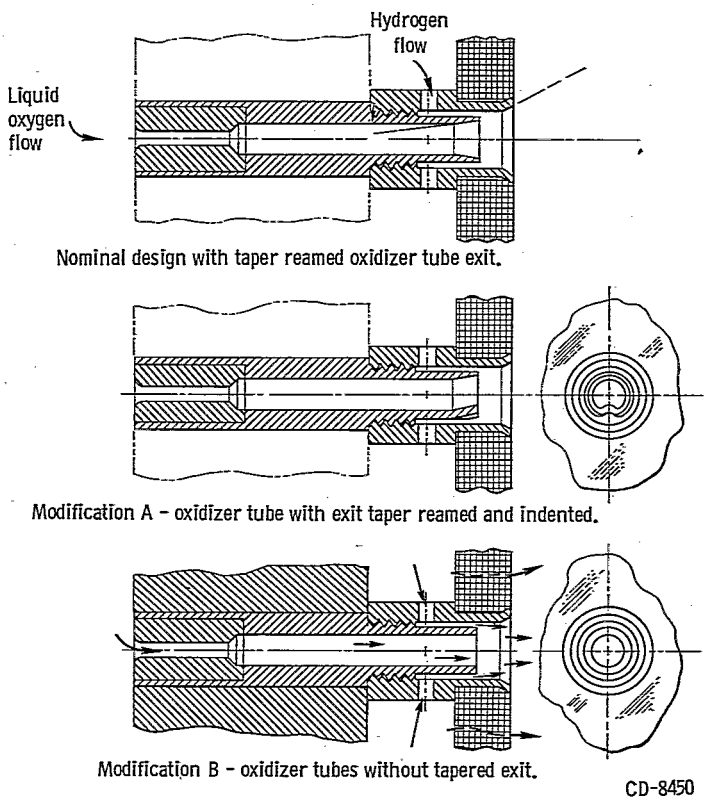

(b) Cross-sectional view of injector elements.

Figure 36. - Injector-element modifications.

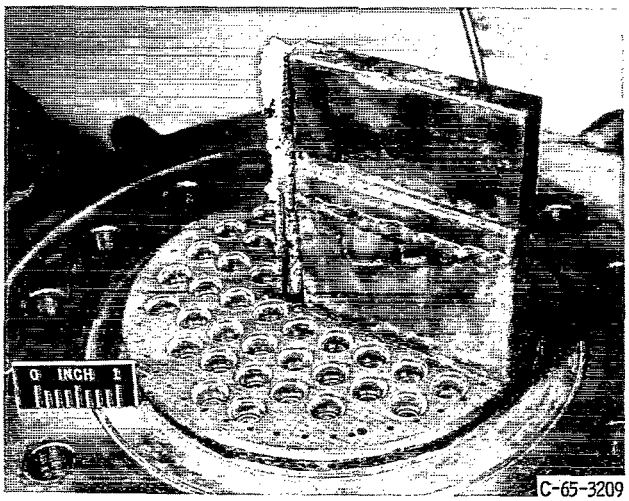

(a) At lower limit of design coolant flow.

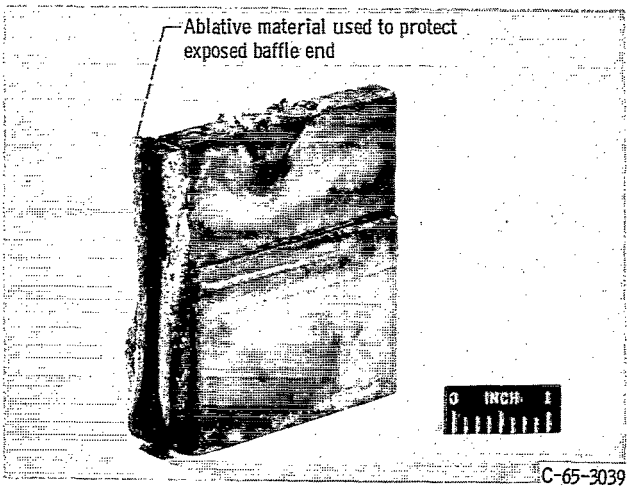

(b) At 80 percent of lower design flow limit.

Figure 37. - Pastfire condition of prototype after 10 seconds of operation.

4.5-inch (0.11-m) diameter ring. Each was bolted to the injector face separately and was fed separately. In the event of damage, or design change, any piece could be individually replaced. As shown, the inner legs and the ring baffles duplicated the subscale test baffle in cross section, and the same cooling flow paths and bolt arrangements were used. The outer leg baffles had a wider base, and, consequently, a different cross-sectional shape. Their design was extrapolated from the inner leg design developed at subscale. At the intersection of radial and circular baffles, a gap of 0.117 inch (0.00297 m) was allowed, as shown in figure 32. This gap is sufficient to allow about 600° F (333° K) differential between the baffle bases and tips without imposition of stress due to restrained thermal growth. Normally, the injector face and the lower part of the baffle would be at nearly equal temperatures, while the baffle tip temperature could rise considerably during a test.

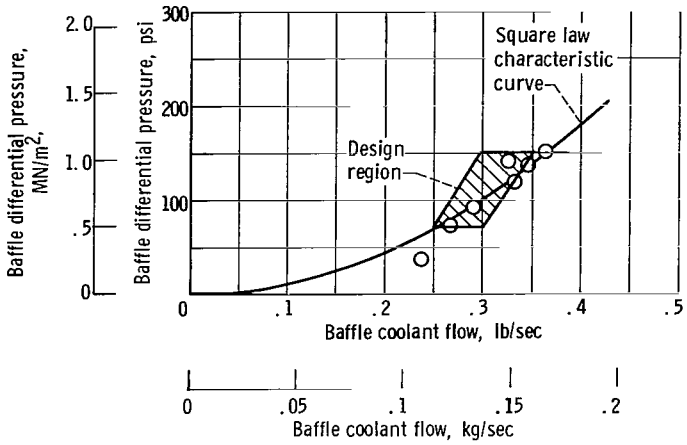

Figure 38. - Flow characteristics of the prototype (copper, convective-film cooled) baffle. Baffle differential pressure corrected to 140° R (78° K) baffle coolant inlet temperature.

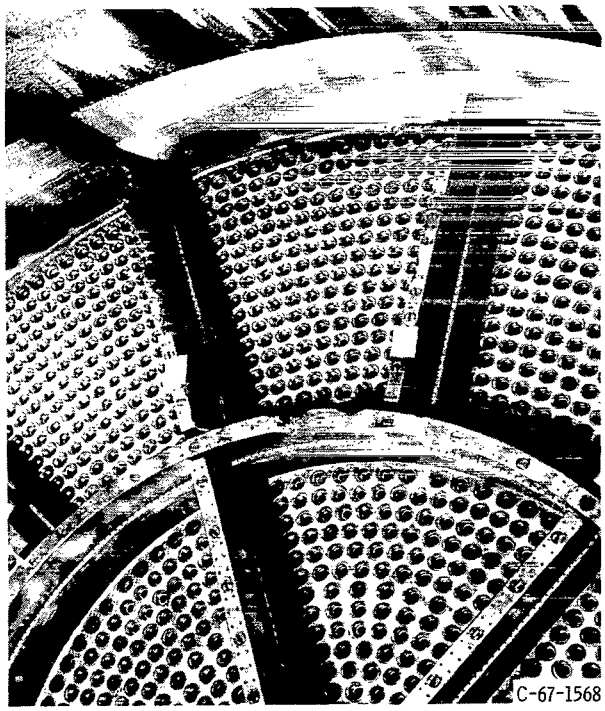

Figure 39. - Postfire condition of full-scale baffle.

The full-scale results indicate that the baffles were effective in attenuating instability. Even during induced unstable operation, pressure excursions were limited to less than 100 psi (0.69×10^6 N/m^2) peak to peak. Later, several tests were made with the baffles removed. The self-triggering temperature was the same as with baffles. However, the amplitude of instability was much higher, with peak pressure excursions over 1000 psi (6.9×10^6 N/m^2). Moreover, injector and chamber damage during induced unstable operation was much more severe. Tests made with and without baffles are compared in reference 14.

The baffles themselves withstood the rigors of full-scale testing quite well. The inner radial baffles were wholly undamaged, although several erosion spots occurred on the outer circular baffle, and substantial erosion occurred on several of the outer radial baffles. Figure 39 shows the injector and baffles after the first full-thrust test at 6.12 O/F. This figure shows the worst damage that occurred during any of the testing. A subsequent test at full thrust and 5.34 O/F did not add to the damage. Most of the erosion on the outer radial legs appeared to be due to inadequate coolant flow. Therefore, after two full-thrust tests, the two most severely eroded outer-radial legs were replaced with new legs which were redrilled to provide approximately 15 percent greater film coolant flow. Further testing showed substantially less damage to these legs, indicating that the higher coolant flow helped.

In general, bolting the baffles to the injector proved quite satisfactory. The baffles remained firmly attached with no apparent bolt loosening during stable operation. This confirmed both the subscale firings and the shake-table tests. Instability did cause baffle loosening; however, it was not difficult to retighten the baffles as necessary between stability tests.

In summary, the subscale development of a baffle-cooling design for the M-1 worked out very satisfactorily. What proved to be a wholly adequate final baffle design was completely established before beginning full-scale tests.

ABLATIVE CHAMBER

Background

Soon after the decision to build the subject M-1 injector, the M-1 engine program was put on phaseout status. Work on the regenerative chamber was stopped. Originally, the initial injector tests were to have been conducted with a film cooled "workhorse" chamber. This would not have allowed accurate performance determination, due to the film cooling flow and the limited duration capabiity of this chamber. These tests were intended to make initial stability and durability investigations. Accurate performance

determination was done later in a regenerative chamber. In view of the phaseout, it was necessary to provide a substitute for the regenerative chamber which would allow an accurate evaluation of performance. The chamber would have to be capable of surviving at least four tests of 3 to 5 seconds full chamber-pressure duration. An extensive study of various techniques for enhancing the duration capability of the workhorse chamber (without film cooling) or of quickly and cheaply completing a convectively cooled chamber was made. The only technique which appeared capable of fulfilling the requirements was ablative cooling. However, there was very little experience of record at conditions near those proposed for the M-1.

Some test data at 1500 psi (10.3×10^6 N/m^2) were available for a small silica phenolic ablative chamber with aluminized hydrazine and nitrogen tetroxide (Titan IIA Subscale; ref. 15). Results were good; only 0.025 inch (0.00064 m) of erosion was experienced after 2 seconds of full pressure operation. Because the combustion temperature was 7000° F (4140° K) and the heat flux on the order of twice that of the M-1 and because general experience showed that ablation rates are lower for hydrogen-oxygen than for earth storable propellants, it appeared that a similar ablative could adequately provide the desired duration capability for the M-1 chamber. When it was assumed that a minimum of 20 seconds total duration was required and that about 0.5 inch (0.013 m) erosion could be safely tolerated, an erosion rate of less than 0.025 inch per second (0.00064 m/sec) would be acceptable. Lewis tests with hydrogen-oxygen at lower chamber pressures showed that a silica reinforcement and phenolic resin binder offered duration capability far superior to a number of other ablative combinations (ref. 16). An ablative chamber design incorporating edge-wrapped silica cloth with a phenolic resin binder was chosen for the initial M-1 injector tests.

Subscale Testing

Ablative nozzles were used for the subscale injector and baffle testing for the same reasons as for full-scale testing. Acceptable convectively cooled chambers were not available in the time framework of the subscale program. Silica-phenolic material similar to that planned for full-scale use was used for three subscale nozzles. Carbon cloth ablative and graphite nozzles were also used, but the silica-phenolic ablative gave the best service. No attempt was made to precisely evaluate the duration capability of the ablatives. However, throat dimensions were taken after each set of tests and a rough measure of erosion rate was made. A complicating factor was the short duration of the tests, most of them being of 1 to 2 seconds duration. Erosion depth expressed as the change in mean throat radius was determined for each nozzle as a function of time. The results for the three silica-phenolic nozzles are shown in figure 40. Nozzles 1 and 2 each

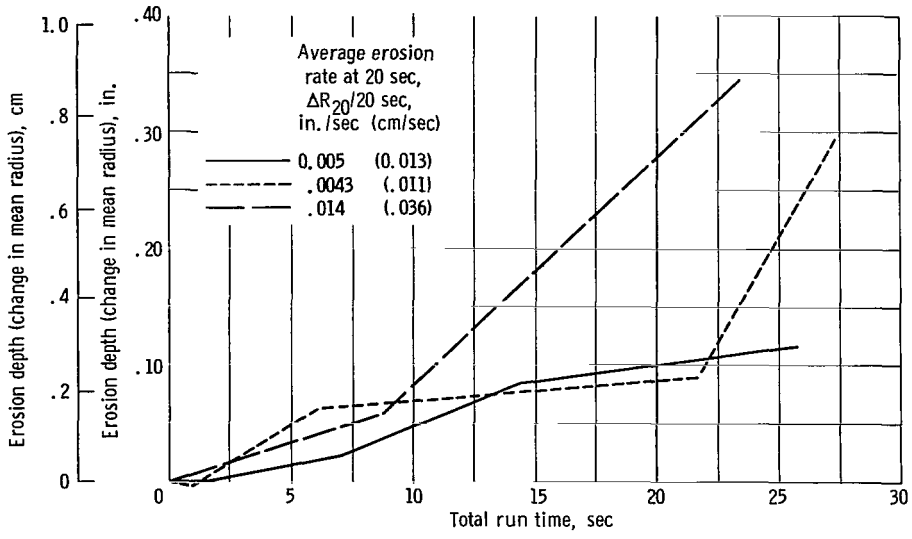

Figure 40. - Erosion rates for M-1 subscale silica-phenolic nozzles.

survived 15 runs, while nozzle three withstood only nine runs. The results indicated that erosion rates well under 0.025 inch per second (0.00064 m/sec) could be expected for the much larger full-scale ablative chamber (32-in. (0.81-m) throat diameter as compared with 4.15-in. (0.105-m)). In fact, erosion rates of less than 0.010 inch per second (0.00025 m/sec) could be expected. The subscale ablative nozzles served well to carry out the subscale injector program. Moreover, the subscale tests clearly indicated that, from the standpoint of erosion resistance, at least, full-scale ablative nozzles could be expected to last substantially beyond the minimum requirements.

Full-Scale Testing

Although the prime objective of full-scale testing was evaluation of the injector, a cursory evaluation of the ablative liners was also made. Two fabrication methods were used in the construction of a prime and backup ablative liner. Both liners used silica-reinforced phenolic material. The primary liner was made using compression molded billets of controlled fiber orientation from which individual rings were cut and later bonded into two conical frustums to form a rough combustion chamber liner. The rough liner assembly was then contour machined on the inside diameter and match machined on the outside diameter to fit with the steel combustion chamber shell. The ablative fibers were oriented downstream at a 35^{o} angle with the chamber centerline. This type of construction was used for the Titan IIA subscale chamber previously described.

The backup liner was built by tape wrapping "net" to a mandrel surface which matched the chamber contour, hydroclave curing the part, contour machining the chamber throat area, and match machining the outside diameter of the liner to fit with the steel chamber shell. The ablative fibers were oriented downstream at approximately 41^{o} with the chamber centerline. This method of liner fabrication is much more commonly used than the former. In general, it can be expected to result in a better ablative liner with less total effort.

Figure 41 shows the full-scale chamber with an ablative liner installed. Each type

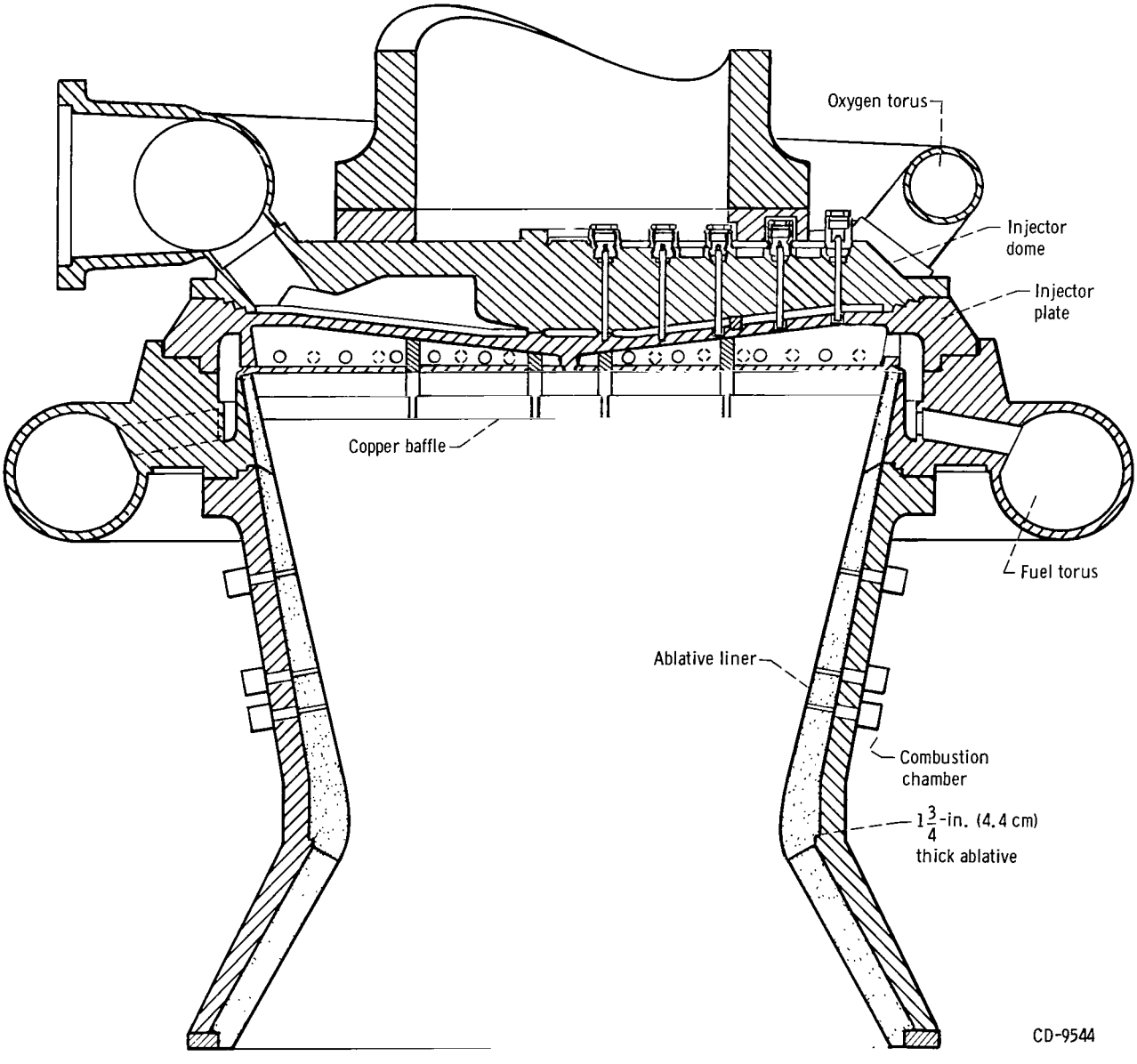

Figure 41. - Full-scale chamber with ablative liner.

of liner was assembled into the shell in three pieces; one piece attached to the fuel torus portion of the chamber, one piece to the upper portion as far as the throat, and one piece to the divergent portion downstream of the throat. Both liners were the same, except that the first liner was built up of segments as previously described. The segmented tail cone section, however, proved defective during fabrication and a tape wrapped tail cone was substituted. The maximum liner thickness was $1\frac{3}{4}$ inches (0.044 m) at the throat. Minimum thickness was 0.84 inch (0.021 m) and occurred at the injector. An ablative silicone rubber compound (RTV-60) was used to bond the liner to the shell and serve as a gas seal at the segment joints.

The ablative liners served their purpose of providing extended duration very well. The first liner was used for 11 full-thrust runs and three partial thrust runs with a total full-thrust duration of 43.5 seconds. Figure 42 shows the throat of this liner after 9 full-

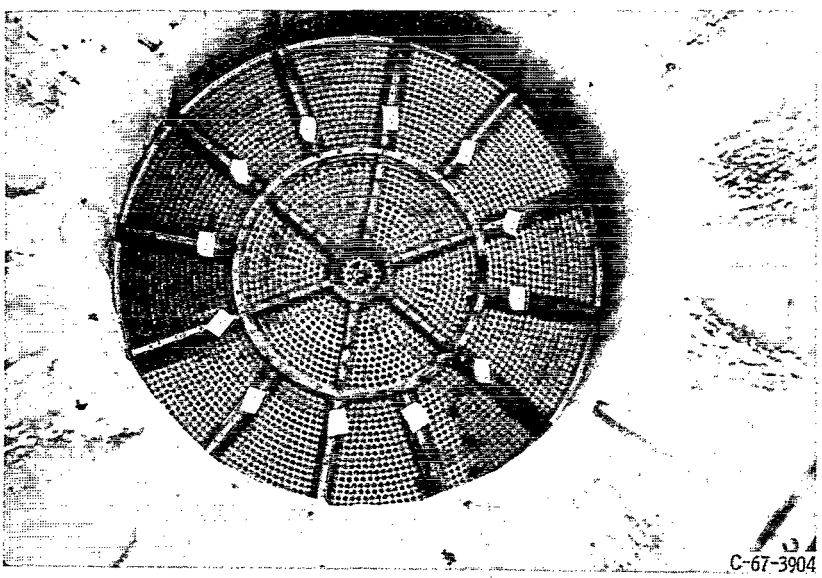

Figure 42. - First ablative liner throat after 9 full-thrust runs. Full-thrust duration, 32.2 seconds; serial number 20 injector.

thrust runs and 32.2 seconds full-thrust duration. Irregular deep gouging can be seen. This appears to be primarily the result of misdirected oxygen streams from the injector. The oxygen-injection tubes made for the first injector (serial number 20) appeared to be generally of poor quality - rough internal surfaces and some nonconcentricity on internal bores. Each element was individually flow checked prior to assembly and the whole injector was flow checked after assembly. The flow tests did not indicate an obvious problem of misdirected streams. Oxygen tubes for the second injector (serial number 12) met requirements on internal finish and concentricity and did not exhibit gouging tendencies during hot firing. Tests of both injectors indicated no significant difference in

performance or stability.

The first liner was operated for two more runs before the tail cone segment broke loose, apparently because of combustion gas getting between it and the shell as a result of a defective gas seal. Both these tests were made to determine stability boundaries. Hence, each operated unstably for several seconds. The average throat erosion (change in radius) at this time was approximately 0.250 inch (0.0064 m). The maximum depth of erosion was 0.84 inch (0.021 m) plus about 0.09 inch (0.002 m) of char. The minimum depth of erosion was 0.11 inch (0.0028 m) plus 0.12 inch (0.0030 m) of char. It was decided to replace the entire liner even though more use could have been derived from upstream segments of the first liner.

The second liner (fabricated by tape wrapping) was tested four times for a total of 31.3 seconds. All four runs were stability boundary tests and each included several seconds of unstable operation. At the conclusion of testing, the liner was in very good condition. It had sustained an average erosion (based on throat diameter measurements) of

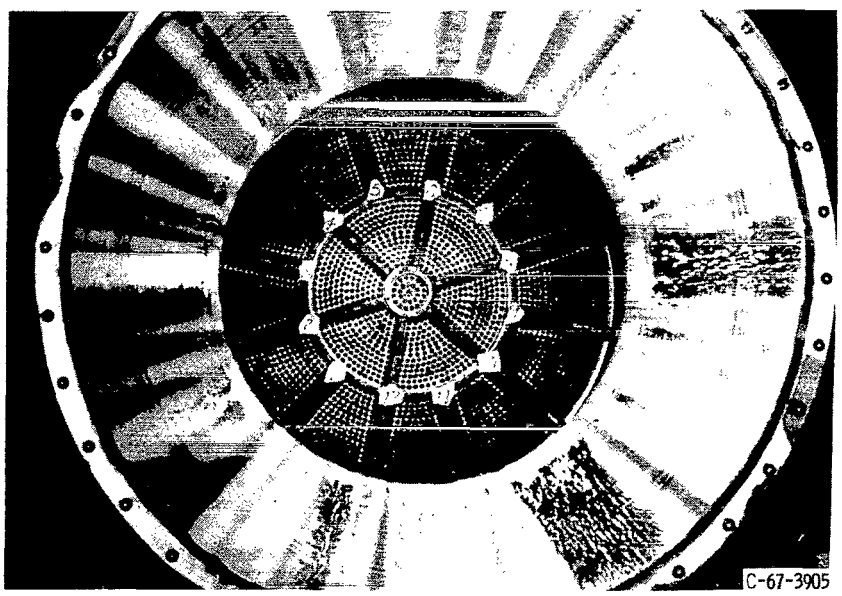

Figure 43. - Second ablative liner after four full-thrust runs. Full-thrust duration, 31.3 seconds; serial number 12 injector.

only about 0.01 inch (0.00025 m). Figure 43 shows the condition of the ablative throat at this time. No substantial gouging is apparent. The injector used (serial number 12) was identical in design to the previous injector (serial number 20); however, it did not have the errant oxygen streams characteristic of the other. The liner appeared to have considerable life left.

Figure 44 shows comparative average erosion figures for both full-scale nozzles and for the three similar subscale nozzles tested. Both full-scale nozzles showed a lower

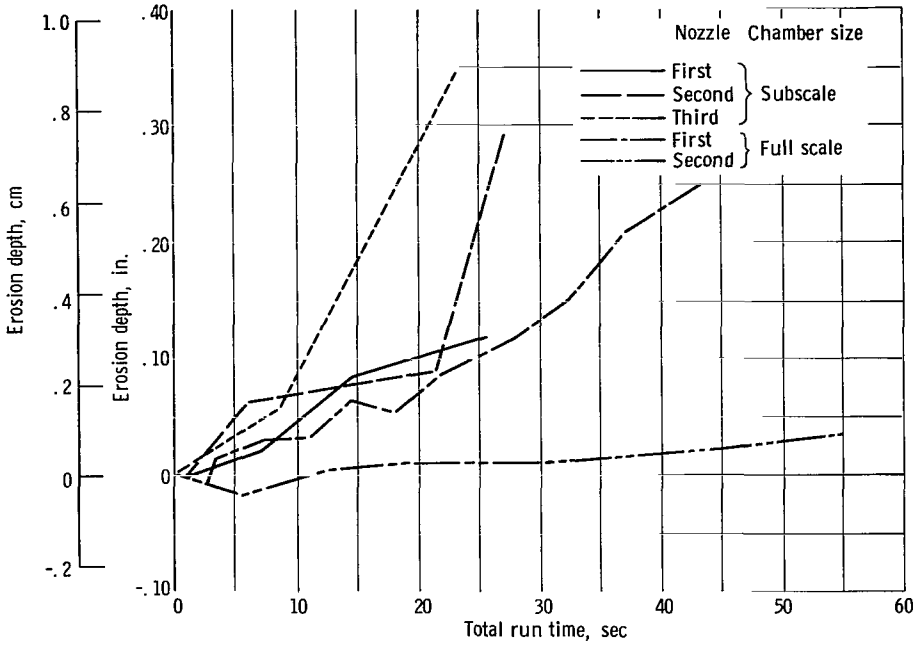

Figure 44. - Comparison of erosion rates for subscale and full-scale M-1 ablative chambers.

erosion rate than the subscale nozzles. The difference in erosion rate is probably primarily a function of diameter (Reynolds number) effects. Surprisingly, the second full-scale nozzle showed considerably less wear than the first (by almost a factor of 10). If the erosion due to gouging is discounted, the erosion rate for the first nozzle is still about five times that of the second. No explicit explanation for this large difference is available. However, it would appear that the injector element characteristics which caused gouging with the first injector may also have contributed to a generally higher boundary-layer mixture ratio and hence higher temperature. Since ablative wear is particularly sensitive to gas temperature in the 3000° to 3600° R (1666° to 2000° K) range, a few hundred degrees difference in boundary-layer temperature due to small injector differences could account for substantial divergence in erosion rate. Physical differences in the two liners (e.g., density, wrap angle, etc.) may also have contributed to the difference in erosion experienced.

START SYSTEM AND IGNITER DEVELOPMENT

Background

The same philosophy used in designing the injector was applied to preparing it for testing. All available data pertinent to facility design, activation, and operation were

collected, analyzed, and brought to bear. Individual components and subsystems were meticulously checked out prior to inclusion in the full system. Analytical studies of critical system problems such as propellant line dynamics and start sequencing were made to guide design and operation. The system design and operating procedures were subjected to critical review by both AGC and Lewis experts prior to actual use. The design of a safe and effective start transient is a good example of this testing philosophy.

The start sequence to be used in testing the injector was carefully studied. Not only was completely new, and very large hardware to be tested, but the test stand itself was newly built and had never been checked out or used. In view of the very high propellant flows required, a bad start could have had calamitous effects, not only on the hardware and stand, but also on the surrounding facilities. The goal, therefore, was to develop a start sequency and ignition source which would ensure safe, reliable starts. The chamber pressure and mixture ratio must be under control throughout the start sequence. The injector and baffle cooling circuits must flow steadily before significant pressure and heat-flux rise takes place. The actual ignition should occur at relatively low pressure and mixture ratio to minimize detonation potential. Too rapid a pressure rise had to be avoided to prevent shock load damage to hardware or test stand.

Start sequences for several rocket thrust chambers are shown in figure 45. The J-2 (200 000-lb (8.9×10^5-N) thrust) and Lewis (20 000-lb (8.9×10^4-N) thrust) hydrogen-oxygen chamber starts are similar. In both cases, tank pressures are set at full steady-state values, the fuel valve is opened first, and the oxygen valve shortly thereafter. The only significant difference is the longer fuel lead used by Lewis. Both starts proceed rapidly from essentially zero to full pressure with the rapid opening of the liquid oxygen valve. The F-1 start (1 500 000-lb (6.7×10^6-N) thrust with RP-1 oxygen), however, proceeds in a stepwise fashion. The whole procedure takes over 3 seconds to establish full thrust. The J-2 takes less than 1/10 of that time. Although the M-1 propellants were the same as for J-2, the M-1 start problems more closely resembled those of the F-1, primarily because of its size. The extremely large valves required (approximately 14 in. (0.36 m)) took longer to operate. Both delay and actual actuation times are longer than for small valves, and flow line volumes are large. The M-1 thrust stand has approximately 18 cubic feet (0.51 m^3) between the main oxygen valve and the thrust chamber. Inertia, transport, and fill times are greater. It was decided that the basic sequential start philosophy of the F-1 was best suited to M-1. Insofar as possible, valves were to operate consecutively rather than simultaneously. This was done to prevent random O/F excursion due to the normal operational tolerances of the large valves. A definite fuel lead was decided on in order to (1) assure full flow of injector and baffle cooling circuits prior to chamber-pressure and heat-flux rise and (2) assure that the ignition and flame propagation would occur at low O/F to minimize the detonation hazard.

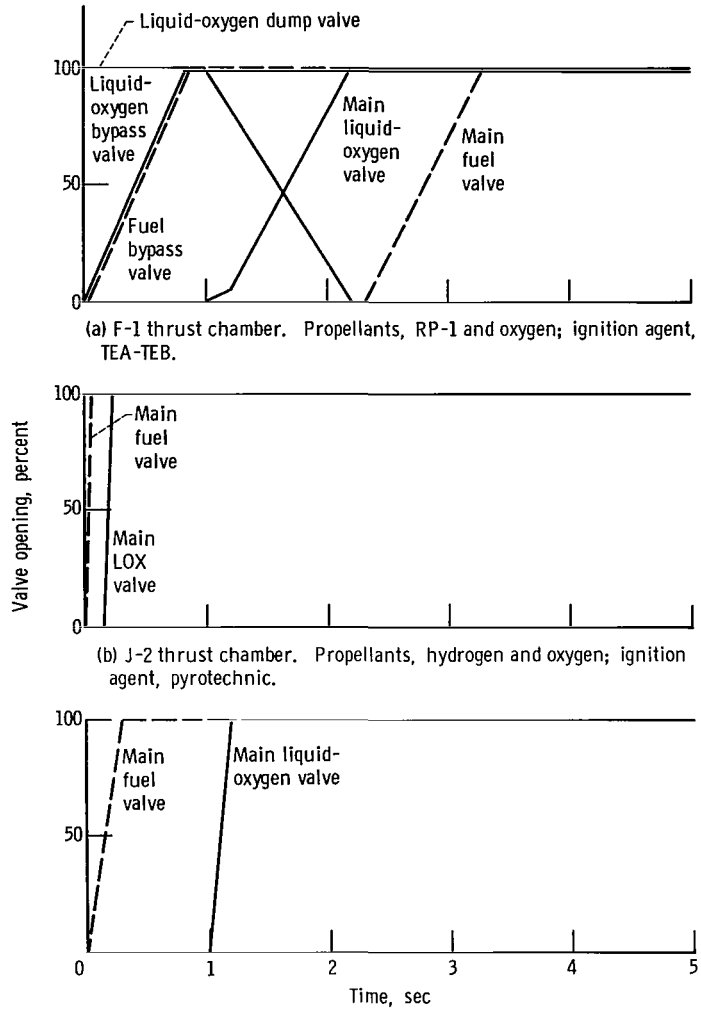

(a) F-1 thrust chamber. Propellants, RP-1 and oxygen; ignition agent, TEA-TEB.

(b) J-2 thrust chamber. Propellants, hydrogen and oxygen; ignition agent, pyrotechnic.

(c) Lewis thrust chamber. Propellants, hydrogen and oxygen; ignition agent, gaseous fluorine.

Figure 45. - Typical start sequences.

A model of the thrust chamber and test stand was set up on an analog computer. Three basic flow control techniques were to be employed: (1) Valve sizing (both main and bypass valves), (2) valve timing (when and at what rate a valve was to be opened), and (3) tank pressures (start at low preset pressures, ramp to final values during transient). Some of the basic ground rules used were: (1) During the flame propagation and initial pressure buildup, O/F was to be greater than 1 but less than about 2.5. (2) The malfunction of any single valve would cause no deleterious effects on chamber or stand; that is, O/F's or pressures would not go out of safe boundaries and a normal shutdown could be made safely after detection of the malfunction. (3) The chamber pressure at ignition

and during flame propagation was to be as low as possible while reasonable minimum flow pressure drops were maintained.

A variety of start sequences was put through the computer. After preliminary selection of a start sequence, various malfunctions were fed into the computer and the effect on the start parameters determined. Necessary adjustments to fit the original ground rules were made. The selected start sequence is shown in figure 46. Propellant tanks prepressures are set at 460 psi (3.2×10^6 N/m^2) for hydrogen, 540 psi (3.7×10^6 N/m^2) for oxygen. The main fuel valve begins to open at a slow rate (2 sec ramp, 0 to 100 per-

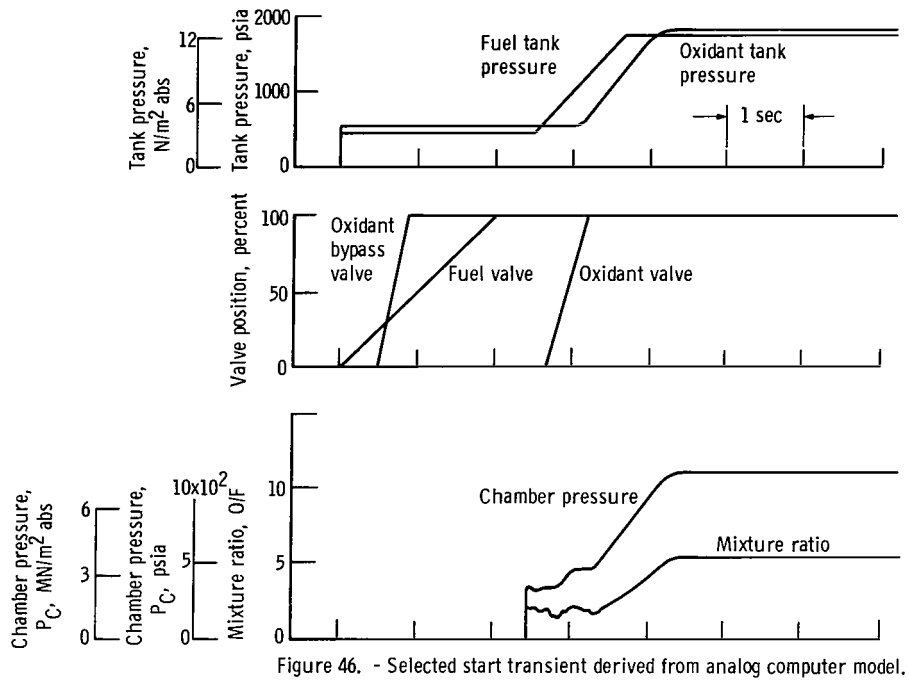

Figure 46. - Selected start transient derived from analog computer model.

cent open). As soon as the fuel valve indicates movement (microswitch at 10 percent open position) a signal is sent to the oxygen bypass valve which opens quickly after a characteristic delay to allow a low flow around the main valve, primarily to fill the volume between the main valve and the injector. In addition, ignition energy is supplied during this period. When the line volume is full, chamber pressure rises quickly (assuming prior ignition). As it passes 200 psi (1.4×10^6 N/m^2) and remains above that value for 100 milliseconds, it signals the fuel tank pressure to start to ramp up to its final level. When tank pressure feedback indicates an increase, the main oxygen valve is allowed to open. As the main oxygen valve passes 50-percent open, the final oxygen tank pressure ramp is initiated. Full thrust is reached approximately 1 second later.

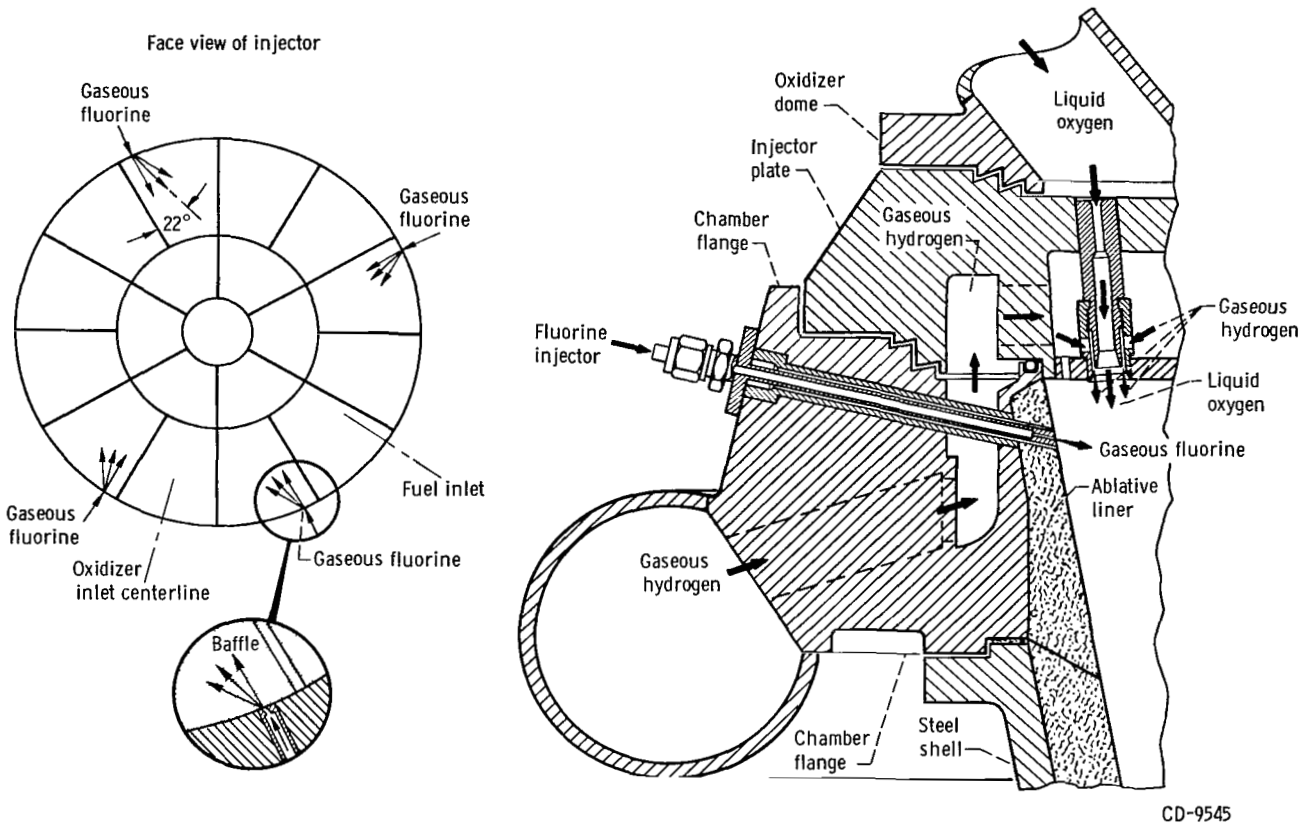

Figure 47. - Fluorine ignition injection system.

Each action in the sequence depends on the prior action for initiation. Should any step in the sequence fail, the sequence stops and shutdown is signalled after an appropriate time. As the figure shows, there are two plateaus of chamber pressure, about 300 psi (2.1×10^6 N/m^2) and about 450 psi (3.1×10^6 N/m^2), prior to the steady-state level of 1100 psi (7.6×10^6 N/m^2). Flow-pressure drops during these plateaus are low, but were judged high enough to limit chugging to a low, essentially safe level. The computer shows that the mixture ratio stays well within the specified limits until the ramp up to steady state. One disturbing aspect of the start was the amount of free hydrogen expelled prior to chamber pressure rise. There was some concern that this much hydrogen (as much as 800 lb (360 kg)) would be a substantial explosion hazard. However, previous experience indicated that little mixing with air would take place prior to ignition and the hydrogen should burn innocuously as a large but "soft" fireball. Therefore, it was concluded that the actual damage would be small. Aerojet also checked this start sequence with its digital computer model. Essentially, the results of the analog studies were confirmed. The sequence was programmed into the analog computer used to operate the thrust chamber test facility.

Although pyrotechnics had been originally planned for ignition, it was decided to change to gaseous fluorine to provide a continuous high-level ignition energy source throughout the start transient for greater reliability. A gaseous fluorine ignition system had been used at Lewis for hydrogen-oxygen thrust chambers since 1958. Several thousand ignitions had been successfully achieved since that time. Reference 17 covers the development of gaseous fluorine ignition for small chambers (approximately 20 000 lb (89 000 N) thrust). Aerojet had also made several successful ignitions during the single element M-1 subscale injector program.

It was decided to bring the gaseous fluorine into the chamber through four instrumentation ports near the injector (fig. 47). The required total flow was extrapolated from the subscale experience. A total flow of approximately 1.5 pounds (0.68 kg) gaseous fluorine per second was selected. This, when burned with hydrogen, was sufficient to give about 60 times the ignition energy supplied by the pyrotechnics. Fluorine was to be supplied to the chamber from the time hydrogen flow started until the beginning of the second chamber pressure plateau. It was to be supplied from a gaseous fluorine tank at approximately 750 psi (5.2×10^6 N/m^2). The tank itself was to be loaded by evaporation from a liquid-fluorine tank just prior to the run. The liquid tank, in turn, was to be filled by condensation under liquid nitrogen from commercial gaseous fluorine bottles. This was done to obtain the requisite high-pressure gaseous fluorine, which was not available in commercial bottles. A schematic of the fluorine preparation and delivery system in shown in figure 48.

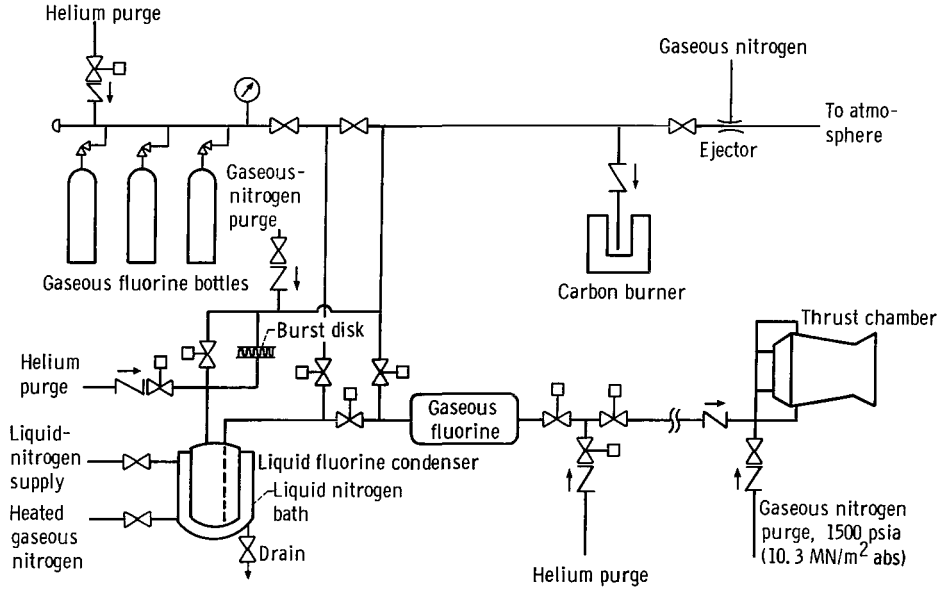

Figure 48. - M-1 gaseous-fluorine preparation and delivery system.

Subscale Testing

Tests were run at Lewis using the existing subscale engine hardware. The five objectives of the tests were (1) To develop the gaseous fluorine injection tube for the full-scale chamber, (2) to evaluate the effect of potential fluorine torching on the copper injector face baffles, (3) to evaluate the effect of fluorine torching on the ablative chamber walls, (4) to evaluate any fluorine-injection-tube damage which might occur during either the engine start transient or the high chamber-pressure conditions after the fluorine flow was cut off, and (5) to evaluate ignition characteristics over a range of fluorine flows. The injection tubes which were evaluated are shown in figure 49.

As illustrated in figure 50, the centerline of the fluorine injection tube for the subscale tests was 0.55 inch (0.015 m) from, and parallel to, the copper injector face baffle, 1.3 inches (0.033 m) downstream from the injector face, and inclined away from it at a 13^{o} angle (conditions simulating the existing ports in the full-scale M-1 thrust chamber). The 22^{o} angle of the tube exit orifice away from the baffle was chosen to maximize the distance along the fluorine streamline before impingement with the injector face baffle of the full-scale chamber. A nominal flow of 0.375 pound per second (0.170 kg/sec) was used for the single injection tube in the subscale tests as this is the nominal flow for each of the four fluorine tubes in the M-1 chamber.

In figure 51, a comparison of the analog-predicted start transient for the full-scale M-1 thrust chamber to the actual start transient obtained for the subscale engine tests is shown. It was most important to closely duplicate the initial combustion chamber pressure and flow relations with time. It may be seen that the subscale chamber pressure and mixture ratio agreed quite closely with the values predicted for the M-1 engine, particularly during the initial plateau period from 2.2 to 2.6 seconds where ignition occurred. The deviations in slope, after the fluorine flow was cut off at 2.65 seconds for the subscale tests, are unimportant because the rest of the run time was important only for the probe durability test objective.

Prior to the first injection tube test (configuration 1, type A in fig. 49), a low-pressure, short-duration, gaseous-fluorine pickling process was used to condition the system. This pickling process was not sufficient as the fluorine burned out the check valves in the feed line. It appeared that the extensive injection tube damage incurred was the result of combustion gas flowing out through the tube after the check valve burnout. A thorough pickling process prior to the next test eliminated the check valve burnout problem. However, the tube used (configuration 2, type B, fig. 49) was burned out early in the second run. It is conjectured that the failure was brought on by a "blow-back" of the contaminant into the fluorine tube by chamber pressure during the first test. This action led to the subsequent fluorine burnout of the tube.

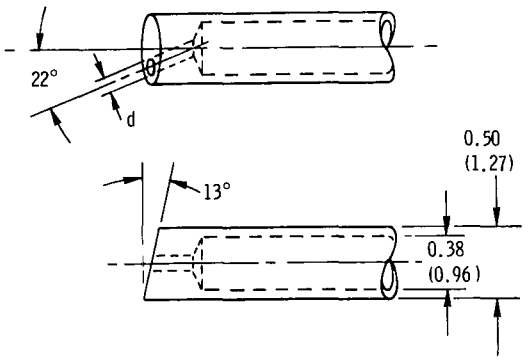

Type A

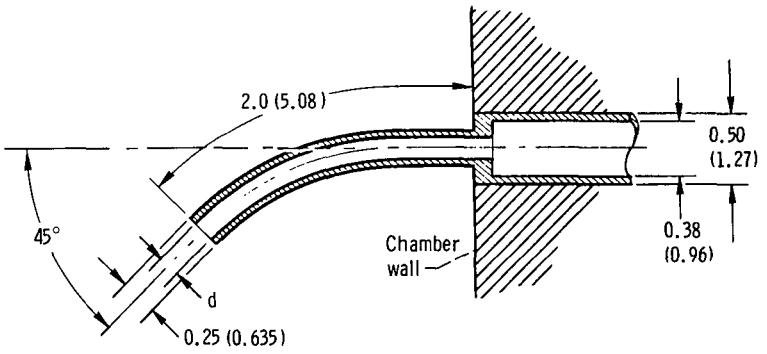

Type C

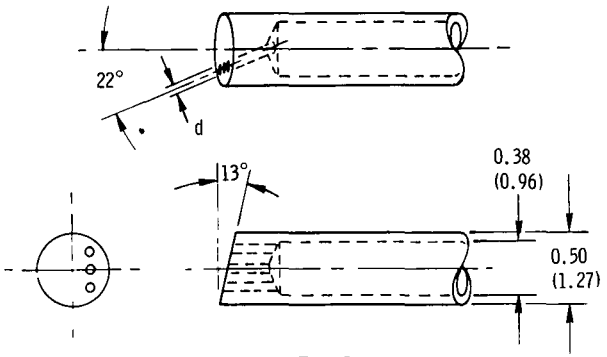

Type B

Configuration	Type	Material	Diameter, d		Method of cleaning		Remarks
			in.	cm	Pickled	Purge	
1	A	Stainless steel	0.159	0.404	No	Low	Destroyed
2	B	Stainless steel	.092	.234	No	Low	Destroyed
3	A	Copper	.159	.404	Yes	High	Good after runs
4	A	Stainless steel	.172	.437	No	High	Eroded at tip
5	C	Stainless steel	.180	.457	--	High	Eroded to 1/2-in. (1.27-cm) length
6	A	Stainless steel	.089	.226	Yes	High	Good after runs
7	A	Copper	.067	.170	Yes	High	Good after runs

CD-9542

Figure 49. - M-1 subscale fluorine injection tubes. (All linear dimensions are in inches (cm).)

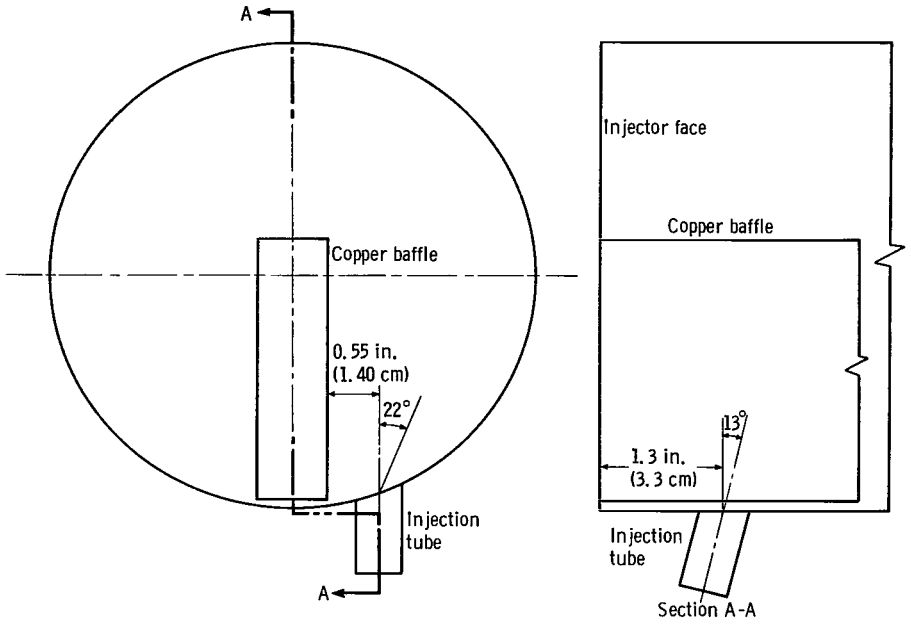

Figure 50. - M-1 subscale fluorine injection tube location.

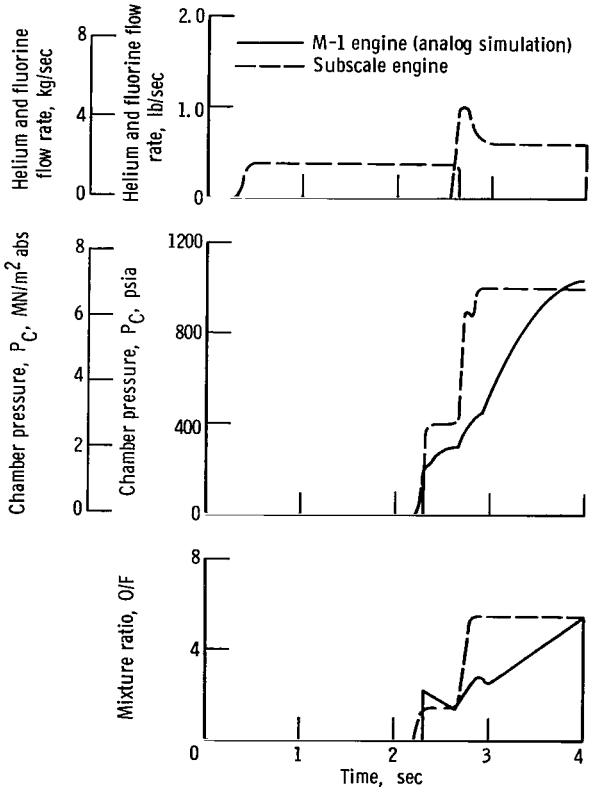

Figure 51. - Start transient comparison.

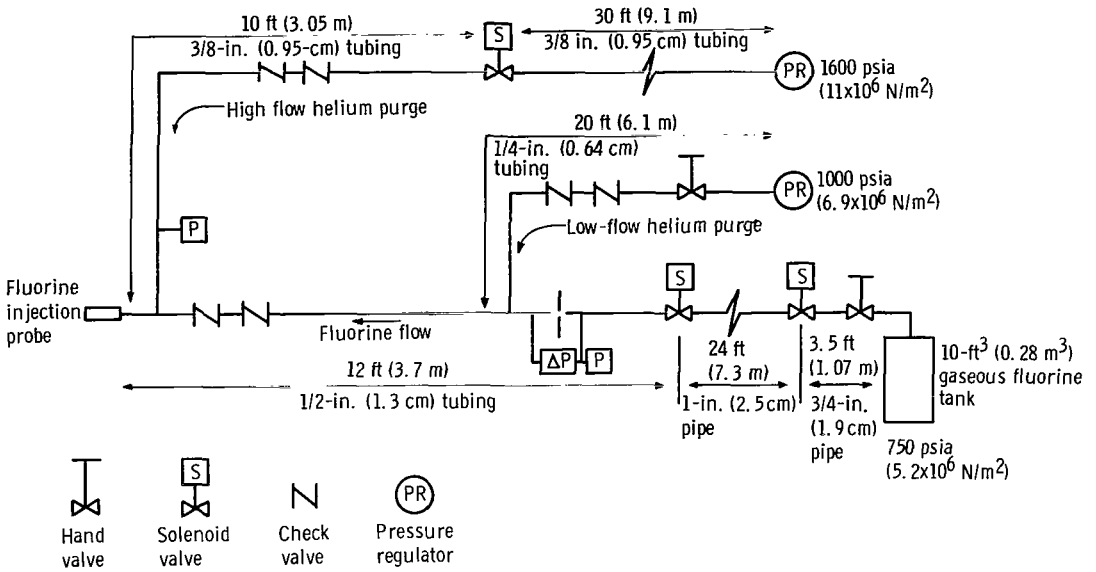

Figure 52. - M-1 subscale fluorine ignition system.

To prevent chamber-pressure blow-back, a high flow purge was timed into the fluorine system. A schematic of the ignition and purge systems is presented in figure 52. With this combination of a thorough pickling and a high-flow purge, the copper tube (configuration 3) ignited the engine satisfactorily and remained undamaged through several start transients and nominal chamber-pressure (1000 psia (6.9×10^6 N/m^2)) tests, including one of approximately 5 seconds duration. After the tests with the copper tube, the stainless-steel tube (configuration 4) was tested. A high-flow purge was employed during this test, but the tube was not pickled. The tube was eroded at the tip from this single run.

Because pickling was the only obvious difference between the copper and stainless-steel tube run conditions, the stainless-steel tube (configuration 6) and the copper tube (configuration 7) were both thoroughly pickled under pressure. After several tests of the stainless-steel tube and two tests of the copper tube, both were in undamaged condition. The fluorine flow and helium purge provided a positive purge through the fluorine injector tube, even during rapid chamber pressure buildup. The system provided a helium purge of approximately 0.06 pound per second (0.027 kg/sec) at 1250 psia (8.6×10^6 N/m^2) to the 0.089-inch (0.0023-m) diameter stainless-steel tube under the choked flow conditions existing before chamber pressure ramped to 1000 psia (6.9×10^6 N/m^2).

The lower flow areas, and correspondingly lower flows, of configurations 6 and 7 were designed to evaluate engine ignition at reduced fluorine flows. Because there are

approximately 200 injector elements in each outer baffle compartment of the full-scale chamber compared with only 51 elements in the subscale chamber, it seemed advisable to test the ignition obtained with this reduced proportion of fluorine to the injected propellant. At a flow of approximately 0.10 pound per second (0.045 kg/sec), ignition was accomplished with tube configuration 6. As an even more stringent test, the fluorine flow was reduced to approximately 0.05 pound per second (0.022 kg/sec) using tube configuration 7. Successful engine starts were achieved at these reduced flows.

The projecting stainless-steel injection tube (configuration 5, type C, fig. 49) was evaluated only as a "dummy" tube (i.e., mounted in the side of the chamber with only purge gas flowing through it) to determine whether it would stand up under combustion conditions in the chamber. The tube was burned off to approximately 1/2 inch (0.013 m) during the first test and eroded very little more during subsequent tests.

The following summarizes the results of the tests: (1) The fluorine appeared to have no detrimental effect on the copper injector face baffle even when tube damage was incurred. (2) The fluorine appeared to have no detrimental effect on the ablative chamber walls. (3) It is definitely necessary to thoroughly pickle the fluorine-injection system, including the tube. (4) A purge of sufficient pressure and flow to prevent "blow-back" during chamber pressure buildup is very desirable, if not necessary, and this purge must be flowing during the run except when fluorine is being injected. (5) Successful subscale engine starts were achieved with flush-mounted chamber wall ignition tubes (type A in fig. 49) at fluorine flows of from near nominal (0.375 lb/sec (0.170 kg/sec)) down to approximately 0.5 pound per second (0.023 kg/sec), indicating that no problem should be experienced in igniting at least the four baffle compartments containing tubes in the full-scale M-1 thrust chamber.

Under similar conditions of pickling and purging, both copper and stainless-steel tubes were undamaged after being used. However, the copper tubes tested appeared to stand up better under severe conditions.

Full-Scale Testing

The approach to testing was to begin cautiously and check out each part of the start transient and start system before proceeding further. The initial firing was programmed to proceed only to the first plateau of chamber pressure. This allowed a checkout of the actual ignition and of the effect of the large hydrogen lead. In addition, the operation of the hydrogen mixer system would be checked out. Because of a concern for safety in disposing very large amounts of free hydrogen, the mixer system had not previously been cold flowed with hydrogen. The mixer is shown in figure 53. It was designed to add gaseous hydrogen to liquid hydrogen in the flow line just downstream of the fuel flowmeter to provide 140° R (78° K) hydrogen at the injector to simulate regenerative chamber opera-

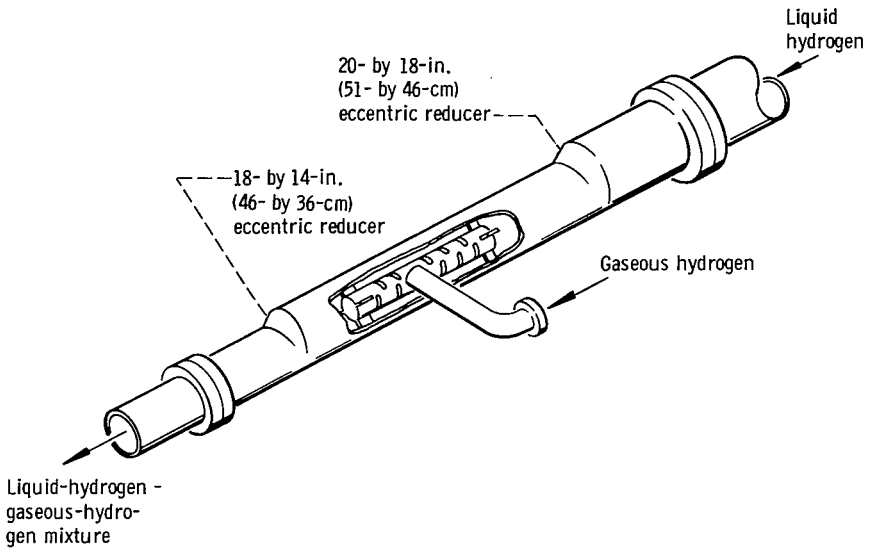

Figure 53. - Gaseous and liquid hydrogen mixer section.

tion. In addition, the system was capable of making smooth variations in temperature between approximately 55° and 160° R (30° and 89° K) for stability testing. The original control system used feedback from the liquid-hydrogen flowmeter to command gaseous-hydrogen flow so as to obtain the desired hydrogen temperature.

The first test demonstrated a smooth ignition, no difficulties with the hydrogen lead, and no hardware damage. However, the hydrogen mixer did not function as planned. Records showed slowdown and reversal of liquid-hydrogen flow immediately after introduction of gaseous hydrogen at the mixer. This resulted in only gaseous hydrogen reaching the injector. Although this was undesirable, it resulted in an excellent view of the injector during ignition due to the transparency of the gaseous hydrogen. High-speed movies, both 400 and 4000 frames per second, were taken through the chamber throat. They showed the ignition sequence in detail. Selected stills from the 4000-frames-per-second motion picture are shown in figure 54. Hydrogen flow started first, followed shortly by fluorine flow. Each fluorine jet appeared on early pictures as a torch burning in the hydrogen atmosphere. The oxygen bypass valve was signalled to open after both the hydrogen and fluorine valves. The first oxygen flow to reach the injector was gaseous and concentrated primarily in the vicinity of the inlet to the oxygen torus. The first frame shown in figure 54 shows ignition of the baffle pocket nearest to the oxygen inlet. A fluorine jet was also in this area (see fig. 47). Oddly, the second frame shows that the flame has gone out. Reignition occurred in the same pocket about 0.22 second later. In general, propagation of the flame appeared to be a function of oxygen distribution rather than of ignition source placement. One compartment ignited from another sequentially around and

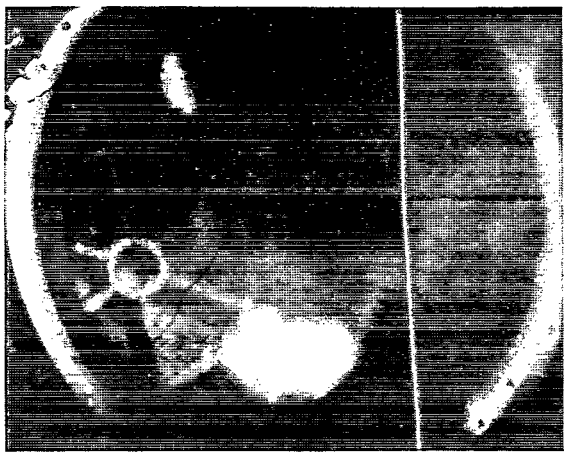

1.235 Seconds

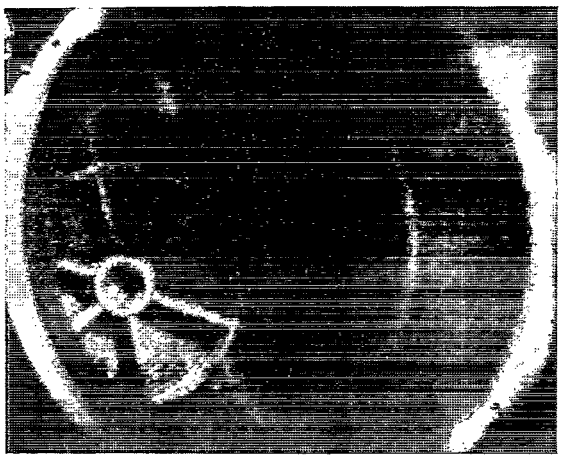

1.434 Seconds

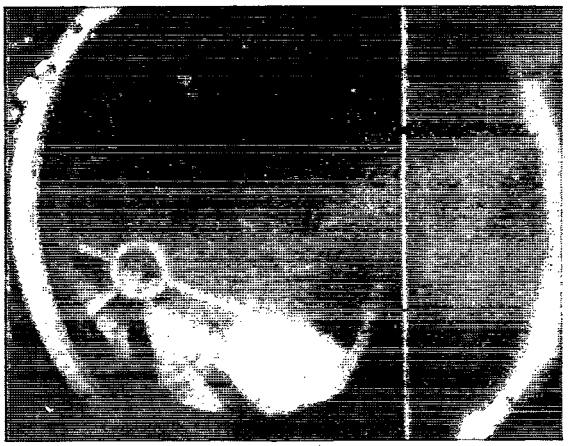

1.68 Seconds

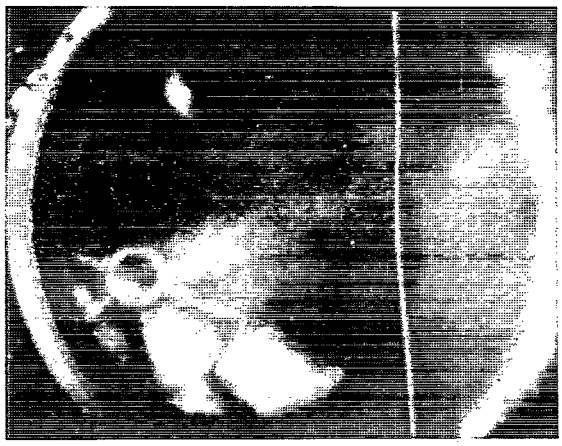

1.8422 Seconds

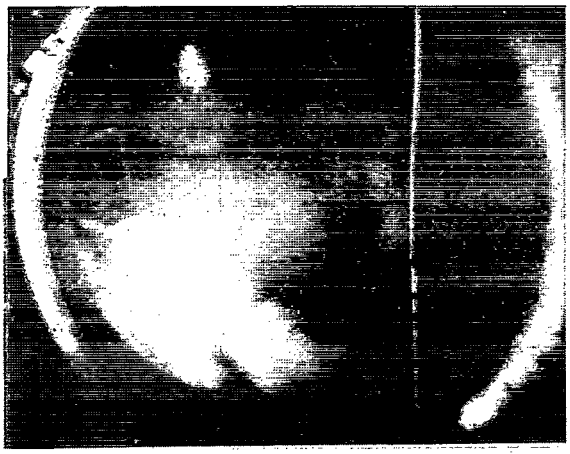

1.8425 Seconds

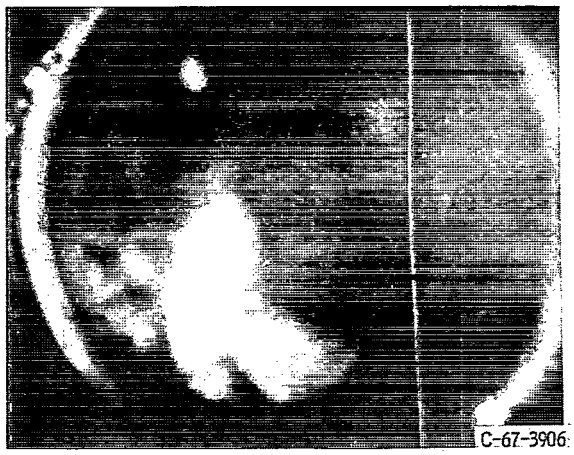

1.885 Seconds

Figure 54. - Ignition sequence. (Fire switch on at time zero).

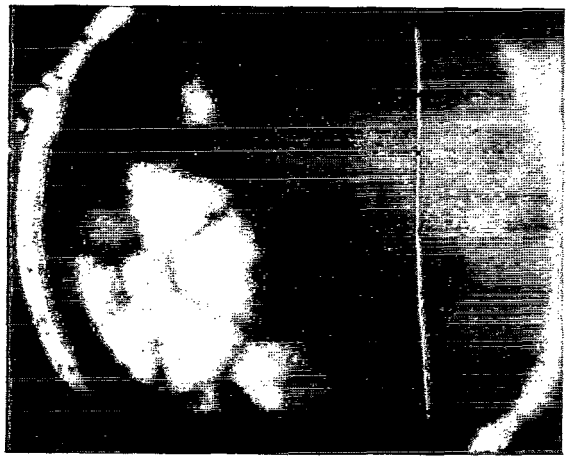

1.940 Seconds

1.9555 Seconds

1.995 Seconds

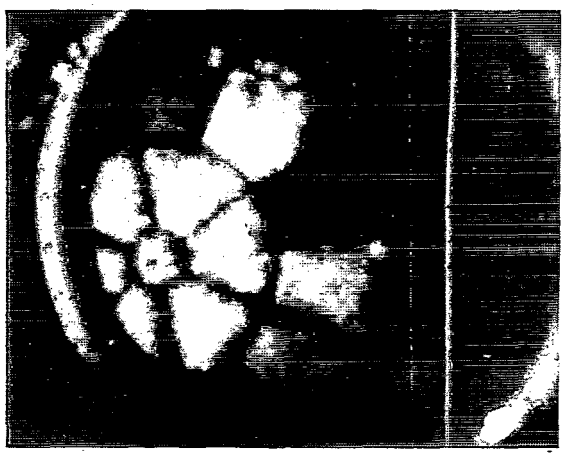

2.04975 Seconds

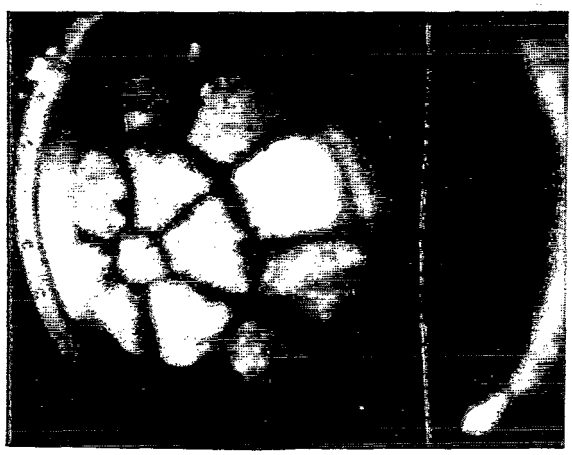

2.065 Seconds

2.302 Seconds.

Figure 54. - Concluded.

into the center of the injector as oxygen flow build up and spread over the injector in sufficient quantity to form a flammable mixture with the hydrogen. It can be concluded from this that a single fluorine jet located near the oxygen inlet would suffice to provide reliable ignition. The flame intensity gradually increased as gaseous (or two phase) oxygen flow to the injector increased. When the oxygen system "hardened" and liquid oxygen was delivered to the injector, intensity very quickly increased.

The mixer problem still needed resolution. Post-run analysis indicated that the mixer gaseous-hydrogen flow would force the column of liquid hydrogen (approximately 20 ft (6.1 m)) between the mixer and the thrust chamber valve through the partly open valve. If the volume rate of gaseous hydrogen addition was greater than the amount of liquid hydrogen which could be forced through the valve, gas pressure at the mixer would rise. This then would restrict liquid-hydrogen flow from the tank. If gaseous hydrogen is added slowly enough, the liquid-hydrogen flow continues, mixing occurs, and a lower density hydrogen reaches the valve which is continuing to open; this allows greater volume flow and greater mixer gas flow. It was calculated that the desired equilibrium hydrogen mixture and temperature conditions for the start transient could be reached in about 1.5 seconds and would occur before chamber-pressure rise to 200 psia (1.4×10^6 N/m^2) with the present start transient.

Because it appeared that the mixer system could be made to work by changing the mode of operation, it was decided to go ahead with the second test which would go to the second chamber pressure plateau (approximately 450 psi (3.1×10^6 N/m^2)). Two attempts proved unsuccessful. It appeared that physical changes to the mixer system were needed to allow successful and reliable operation. An analog model of the mixer itself was set up at Lewis. Results showed flow reversals and oscillations similar to those observed on the test stand. Inputs were varied based on other analyses to determine fixes. The model showed that additional pressure drop in the liquid-hydrogen flow line upstream of the mixer was desirable. It also showed that initial steps in gaseous-hydrogen flow would cause liquid-hydrogen flow stoppage under virtually any condition. Increased liquid-hydrogen pressure drop quickly damped the flow oscillation, but did not completely prevent it when a step in gaseous hydrogen flow was applied. Delaying opening of the gaseous-hydrogen valve until the liquid-hydrogen valve is further open did reduce the amount of flow disturbance caused by a step in gaseous-hydrogen flow. The analog model and other analyses indicated the following changes as desirable in preventing mixer flow oscillations:

(1) Increased flow resistance in liquid-hydrogen flow line between tank and mixer. (Approximately 100 psi (0.69×10^6 N/m^2) increase in ΔP.)

(2) Decreased mixer gaseous-hydrogen pressure drop

(3) Smooth ramp of mixer gaseous-hydrogen flow from zero to prescribed value

(4) Introduction of initial gaseous-hydrogen mixer flow as late as possible (to allow fuel valve to open further and decrease downstream resistance). This, of

course, was limited by the imposed requirement for relatively warm hydrogen (at least 100° R) (55° K)) during combustion. Although a higher temperature would have been desirable, 100° R (55° K) was judged (prior to testing) to give reasonable assurance of stability.

Two physical changes were made to the fuel flow system to improve mixer operation. Increased resistance upstream of the mixer was provided by restricting the fuel safety valve motion to 25 percent of full stroke. Approximately 40 square inches (0.026 m^2) of open area was added to the downstream side of the mixer gasous hydrogen inlet to decrease gas flow pressure drop and velocity. Fuel preset tank pressure was increased to 650 psi (4.5×10^6 N/m^2) to compensate for the added pressure drop through the fuel safety valve. Operational changes to dalay the start of gas flow and to introduce it with a smooth ramp buildup were made.

The next attempt to continue the start transient through the second plateau of chamber pressure was shut down prematurely by excessive hydrogen temperature at the entrance to the fuel valve, which indicated inadequate liquid flow. Examination of the records showed a higher pressure drop through the fuel safety valve than had been expected. This caused the too-low fuel flow. Fuel tank prepressure was increased to 800 psia (5.5×10^6 N/m^2) for the next test which was completely satisfactory in all respects. The mixer worked perfectly, delivering the desired hydrogen temperature at all stages. All valves and controls operated as programmed. No hardware or facility damage was observed. The supposed problem of excessive free hydrogen during the start offered no difficulties. It ignited smoothly to produce a large, generally spectacular, but innocuous fireball. With all systems and hardware now checked out and working as planned, the next step was to proceed through the whole start to full-pressure operation. This was done successfully, corroborating the extensive testing and analysis that proceeded this operation. Figure 55 shows a comparison of the analog predicted start transient (chamber pressure and mixture ratio) with a typical actual start transient. They compare quite well. Deviations are due to differences between assumed and actual physical characteristics of the system and setup changes made to accommodate the mixer problems uncovered after the analog analysis was completed. For example, the lower than predicted mixture ratio was probably due to the higher fuel preset tank pressure (800 psi (5.5×10^6 N/m^2) as compared with 460 psi (3.2×10^6 N/m^2)), which was introduced to accommodate to hydrogen mixer requirements.

Throughout these and later tests, the Lewis developed fluorine-injection probes worked perfectly. They neither sustained nor caused damage. The fluorine ignition system itself also operated very well. The only instance of difficulty was that the fluorine valve failed to open once during a start because of a defective pilot valve. This caused no problem, because the sequential start system could not continue without the fluorine valve opening. The test was shut down by the safety system after proceeding for 1.35 seconds

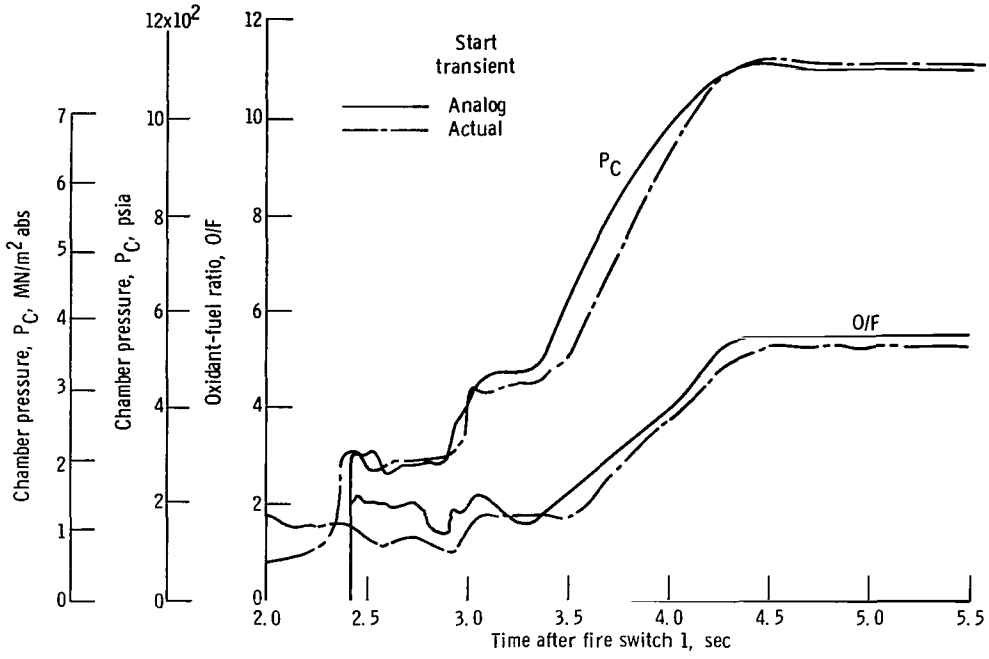

Figure 55. - Comparison of analog and actual start transient.

without ignition. This was the only shutdown caused by the safety system during the full-thrust test series. Several shutdowns were initiated by the safety system during a partial thrust series. These were all based on actual conditions. In summary, the start transient developed on the analog computer and the start system derived from it well fulfilled their intended function.

Careful preliminary testing of all the start system components and functions prior to commitment to full-thrust operation contributed greatly to the successful and safe operation of this program. The meticulous planning and painstaking implementation throughout the facility preparation, activation, and initial testing is described in reference 18.

CONCLUDING REMARKS

The M-1 injector development demonstrated that rational design can be successfully employed for large hydrogen-oxygen injectors and that laborious and costly cut and try procedures are not necessary. Specifically, during the first full-thrust test with the injector and chamber, the development goals of high combustion efficiency, stable operation, and hardware integrity were all demonstrated satisfactorily.

The philosophy employed in the M-1 injector development included the following specific elements:

1. Available data for each step in the design process were collected and analyzed. Full use was made of all pertinent experience and available theory to lay the foundations of design. For example, the very successful J-2 injector design was arrived at after years of assiduous effort to overcome some of the same problems that the M-1 had to face. There was no need to retrace that difficult path. The basic J-2 injector concept was chosen and existing research data were used to update and adapt it to M-1 requirements.

2. Where existing data did not provide an adequate basis for design, small-scale testing was utilized to provide additional data before commitment to full-scale hardware. This was done for the M-1 baffle cooling design and proved quite successful in producing an acceptable design at minimum cost.

3. In cases where subscale testing could not provide the required information in a reasonable time or cost framework, analytical simulations of a specific problem was used to provide guidance. A case in point was the M-1 start transient, which was developed with an analog simulation of the test stand and hardware. The smooth, safe, predictable starts achieved during full-scale testing confirmed the validity of this approach.

4. In the development process, including decision making and implementation, the highest level of technical competence in industry and government was combined and brought to bear on the problems.

Unfortunately, there are cases where even the best preparations fail to provide assurance of complete success. For example, all the prior experience, subscale testing, and analysis did not allow the confident prediction of acoustic stability margin. In this case, the approach was to incorporate all feasible techniques for improving stability and to determine the actual margin achieved through full-scale testing. The prior extensive analysis and testing provided the confidence to proceed to full-scale testing with reasonable assurance that the tests would be successful and that the program goals would be achieved. The successful testing of the M-1 injector validated this confidence.

SUMMARY OF RESULTS

1. Injector performance goals were met. Combustion efficiency was 96 percent at rated conditions. An extrapolation of sea-level data to vacuum conditions gave a specific impulse of 429.5 pounds force second per pound mass (4212 N-sec/kg) which is equivalent to the PFRT contract specification. The injector operated stably under normal operating conditions; stability evaluation tests at lower hydrogen-injection temperatures showed considerable margin. The self-triggering temperature was approximately 78° R (43° K) as compared with a normal engine operating temperature of 140° R (78° K).

2. The baffle design, which had been developed through subscale testing, was successfully applied to the full-scale injector and showed excellent durability.

3. The ablative chambers also showed excellent durability. The first had an average throat erosion of approximately 0.250 inch (0.0064 m) in 43.5 seconds of full-thrust testing. This, however, included substantial gouging caused by injector anomalies. The second chamber, run with an improved injector, exhibited throat erosion of only about 0.01 inch (0.00025 m) in 31.3 seconds of full-thrust testing with no gouging.

4. The start transient which was developed on the analog computer was essentially duplicated during actual testing. In combination with the gaseous-fluorine ignition system, it provided consistently smooth, repeatable, safe starts.

Lewis Research Center,
National Aeronautics and Space Administration,
Cleveland, Ohio, October 13, 1967,
726-46-00-01-22.

REFERENCES

1. Wanhainen, John P.; Parish, Harold C.; and Conrad, E. William: Effect of Propellant Injection Velocity on Screech In a 20,000-Pound Hydrogen-Oxygen Rocket Engine. NASA TN D-3373, 1966.

2. Priem, Richard J.; and Heidmann, Marcus F.: Propellant Vaporization as a Design Criterion for Rocket-Engine Combustion Chambers. NASA TR R-67, 1960.

3. Hersch, Martin: A Mixing Model for Rocket Engine Combustion. NASA TN D-2881, 1965.

4. Summerfield, Martin: A Theory of Unstable Combustion in Liquid Propellant Rocket Systems. ARS J., vol. 21, no. 5, Sept. 1951, pp. 108-114.

5. Drain, Daniel I.; Schum, Harold J.; and Wasserbauer, Charles A.: Relations of Combustion Dead Time to Engine Variables for a 20,000-Pound-Thrust Gaseous-Hydrogen - Liquid-Oxygen Rocket Engine. NASA TN D-851, 1961.

6. Hannum, Ned P.; and Conrad, E. William: Performance and Screech Characteristics of a Series of 2500-Pound-Thrust-Per-Element Injectors for a Liquid-Oxygen-Hydrogen Rocket Engine. NASA TM X-1253, 1966.

7. Reardon, Frederick H.: Combustion Stability Characteristics of Liquid Oxygen/Liquid Hydrogen at High Chamber Pressures. Paper No. 65-612, AIAA, June 1965.

8. Scott, Herbert E.; Bloomer, Harry E.; and Mansour, Ali H.: M-1 Engine Subscale Injector Tests. NASA TN D-4053, 1967.

9. Sievers, Gilbert K.; Tomazic, William A.; and Kinney, George R.: Theoretical Performance of Hydrogen-Oxygen Rocket Thrust Chambers. NASA TR R-111, 1961.

10. Wenzel, Leon M.; and Szuch, John R.: Analysis of Chugging in Liquid-Bipropellant Rocket Engines Using Propellants with Different Vaporization Rates. NASA TN D-3080, 1965.

11. Crocco, Luigi; and Cheng, Sin-I: Theory of Combustion Instability in Liquid Propellant Rocket Motors. AGARDograph 8, Butterworths Scientific Publications, 1956.

12. Reardon, H.: M-1 Thrust Chamber Transverse Mode Combustion Stability Analysis. Rep. No. TCR 9621-012, Aerojet-General Corp., 1963.

13. Conrad, E. William; Wanhainen, John P.; and Curley, Jerome K.: Cooled Baffle Development for M-1 Engine Using a Subscale Rocket Engine. NASA TM X-1267, 1966.

14. Datsko, Steve C.; and Tomazic, William A.: Stability and Performance Comparison of the M-1 Injector With and Without Baffles. Paper presented at Fourth ICRPG Comb. Conf., October 1967.

15. Williams, Ray J.; Mueggenburg, Harry H.; Sabiers, Ralph; Leymaster, I. L.; and England, C. L.: Full-Scale Breadboard Engine and Components. Vol. 4 of Improved Titan Predevelopment. (AFBSD-TR-65-455, Vol. 4, DDC No. AD-370150), Aerojet-General Corp., Feb. 1966.

16. Salmi, Reino J.; Wong, Alfred; and Rollbuhler, Ralph J.: Experimental Evaluation of Various Nonmetallic Ablative Materials as Nozzle Sections of Hydrogen-Oxygen Rocket Engine. NASA TN D-3258, 1966.

17. Straight, David M.; and Rothenberg, Edward A.: Ignition of Hydrogen-Oxygen Rocket Engines with Fluorine. NASA TM X-101, 1959.

18. Clark, D. H.: Activation and Initial Test Operations of Large Rocket Engine-Thrust Chamber Test Facilities. Paper No. 67-455, AIAA, July 1967. (Also available as NASA CR-72300.)

NASA-Langley, 1968 — 28 E-3882

"The aeronautical and space activities of the United States shall be conducted so as to contribute . . . to the expansion of human knowledge of phenomena in the atmosphere and space. The Administration shall provide for the widest practicable and appropriate dissemination of information concerning its activities and the results thereof."

—NATIONAL AERONAUTICS AND SPACE ACT OF 1958

NASA SCIENTIFIC AND TECHNICAL PUBLICATIONS

TECHNICAL REPORTS: Scientific and technical information considered important, complete, and a lasting contribution to existing knowledge.

TECHNICAL NOTES: Information less broad in scope but nevertheless of importance as a contribution to existing knowledge.

TECHNICAL MEMORANDUMS: Information receiving limited distribution because of preliminary data, security classification, or other reasons.

CONTRACTOR REPORTS: Scientific and technical information generated under a NASA contract or grant and considered an important contribution to existing knowledge.

TECHNICAL TRANSLATIONS: Information published in a foreign language considered to merit NASA distribution in English.

SPECIAL PUBLICATIONS: Information derived from or of value to NASA activities. Publications include conference proceedings, monographs, data compilations, handbooks, sourcebooks, and special bibliographies.

TECHNOLOGY UTILIZATION PUBLICATIONS: Information on technology used by NASA that may be of particular interest in commercial and other non-aerospace applications. Publications include Tech Briefs, Technology Utilization Reports and Notes, and Technology Surveys.

Details on the availability of these publications may be obtained from:

SCIENTIFIC AND TECHNICAL INFORMATION DIVISION

NATIONAL AERONAUTICS AND SPACE ADMINISTRATION

Washington, D.C. 20546